



HAL
open science

Reduced model for fracture of geometrically exact planar beam: Non-local variational formulation, ED-FEM approximation and operator split solution

Adnan Ibrahimbegovic, Rosa-Adela Mejia-Nava, Suljo Ljukovac

► To cite this version:

Adnan Ibrahimbegovic, Rosa-Adela Mejia-Nava, Suljo Ljukovac. Reduced model for fracture of geometrically exact planar beam: Non-local variational formulation, ED-FEM approximation and operator split solution. *International Journal for Numerical Methods in Engineering*, 2023, 125, pp.e7369. 10.1002/nme.7369 . hal-04414964

HAL Id: hal-04414964

<https://hal.science/hal-04414964v1>


Submitted on 24 Jan 2024

HAL is a multi-disciplinary open access archive for the deposit and dissemination of scientific research documents, whether they are published or not. The documents may come from teaching and research institutions in France or abroad, or from public or private research centers.

L'archive ouverte pluridisciplinaire **HAL**, est destinée au dépôt et à la diffusion de documents scientifiques de niveau recherche, publiés ou non, émanant des établissements d'enseignement et de recherche français ou étrangers, des laboratoires publics ou privés.

RESEARCH ARTICLE

Reduced model for fracture of geometrically exact planar beam: Non-local variational formulation, ED-FEM approximation and operator split solution

Adnan Ibrahimbegovic^{1,2}  | Rosa-Adela Mejia-Nava¹ | Suljo Ljukovac¹

¹Chair of Computational Mechanics, University of Technology Compiègne, Alliance Sorbonne University, Compiègne, France

²IUF, Institut Universitaire de France, Paris, France

Correspondence

Adnan Ibrahimbegovic, Chair of Computational Mechanics, Laboratoire Roberval de Mécanique, Centre de Recherche Royallieu, University of Technology Compiègne, Alliance Sorbonne University, 60200 Compiègne, France.

Email: adnan.ibrahimbegovic@utc.fr

Summary

In this work, we present a novel reduced model for computing the solution to a bending fracture problem of the geometrically exact beam. The Reissner model is chosen for representing the large elastic and large plastic deformations of such a beam model. The non-local variational formulation is proposed to deal with the softening phenomena characteristic of fracture. The fracture energy is introduced as the main fracture parameter, rather than (in general) ill-defined characteristic length used for previous non-local models. The discrete approximation is built in terms of the embedded-discontinuity finite element method (ED-FEM), which needs no initial crack for optimal performance nor detailed crack kinematics description, such as in the X-FEM or the phase-field approach. This kind of approach builds upon the best approximation property of the FEM discrete approximation in the energy norm and provides the best-approximation property for the dissipated energy computations, and thus optimal computational accuracy if the quantity of interest is inelastic dissipation. The computations are carried out by the operator split method, which separates the computations of global state variables (displacements and stress) from local (internal) variables including the crack opening. Several illustrative examples are provided to confirm an excellent performance of the proposed methodology.

KEYWORDS

embedded-discontinuity discrete approximation, fracture, geometrically exact beam, non-local variational formulation, operator split solution procedure, planar deformation

1 | INTRODUCTION

In this work we seek to provide a novel reduced model for fracture of slender structures in planar deformation that can be represented by the geometrically exact beam. The traditional approach to fracture of beams is based upon the concept of a 'plastic hinge', where one assumes the load-bearing capacity of a particular beam cross-section to be limited to plastic moment M_y , and the limit load analysis is performed as an event-to-event strategy introducing the corresponding releases to transform the beam stiffness matrix.¹ A more consistent approach to obtain a reduced beam model with stress resultant plasticity² can represent the 3D solid mechanics computational results with both hardening and softening phase of large plastic deformation, instability and fracture. However, the reduced model² is proposed only in the framework of

small displacement gradient theory. For improved prediction of final failure mechanisms, it is also necessary to include geometric non-linearities. This is presented in this paper in the framework of the geometrically exact beam theory of Reissner.³ We finally note that although the reduced model approach is currently attracting a lot of attention of research community (e.g., see References 4,5), not much is oriented towards localized failure and fracture, apart a mesh coarsening approach.⁶

The main novelties with respect to several alternative models for fracture⁷ are as follows. The proposed approach is cast in stress resultant format, relying upon multiplicative decomposition of the beam deformation gradient that can accommodate both large elastic and large plastic strains, contrary to earlier rate-type formulations based upon an additive decomposition of the strain rate.⁸ We also go one step further and provide the formulation that can handle the phenomena of localized failure with fracture of the geometrically-exact beam* by proposing a non-local variational formulation, where the fracture parameter is the fracture energy rather than the so-called characteristic length, which is typical of earlier non-local approaches to fracture.^{11,12} The same choice is also made in the phase-field formulation of fracture,^{10,13} by using the global representation of crack and generalizing the Griffith linear fracture mechanics theory.¹⁴ However, the ED-FEM discrete approximation proposed herein needs no pre-existing crack nor it seeks the crack kinematics representation, such as for the phase-field¹⁰ or the X-FEM approach to fracture,¹⁵ but rather employs the embedded discontinuity finite element representation that provides the best approximation to dissipated energy in the spirit of the best approximation property of the finite element method.¹⁶ In addition to this advantage in providing the optimal performance in discrete approximation to fracture problems, it also uses the fracture energy as the most reliable model parameter for quantifying the fracture of a particular material.

In the formulation of the proposed beam element we use as the starting point our previous work¹⁷ that reduced the geometrically nonlinear solid mechanics formulation⁷ to stress-resultant geometrically exact beam for elastic case. This is here extended to stress resultant plasticity formulation that can accept any plasticity criteria⁸ written directly in terms of axial force, shear force and bending moment and carry on with softening phase until complete failure and fracture. The evolution equations for internal variables, here represented by the plastic part of beam strain measures for axial, shear and bending, are developed in rate form, by using the appropriate form of the maximum plastic dissipation principle.^{7,18} Subsequently, when the beam model has reached the ultimate capacity of a cross-section, we activate one of three failure modes in either bending moment, shear or axial force, with a non-linear softening response. For simplicity, we keep failure modes uncoupled assuming that only one softening failure mechanism can be activated at a time. In a recent work¹⁹ we presented displacement discontinuity failure modes (mode I or mode II), whereas in this work we focus upon bending localized failure and fracture of beams. The softening phenomena lead to corresponding localized plastic deformations, with either curvature, shear or axial strain reducing to a narrow domain (or a 'hinge point') with high strain gradients, which requires special interpolation.⁷ In discrete approximation, the failure mode is represented by a field discontinuity and placed within the framework of the incompatible-mode method.²⁰ This allows us to provide the robust computational procedure based upon of operator split, which separates the global computations of state variables (displacements and rotations providing beam strains) versus local computations of internal variables (plastic strains and curvatures). Such an operator split procedure is a more robust than the one provided by X-FEM fracture model when using structured mesh for heterogeneous structures where one should introduce both displacement/rotation discontinuity (representing fracture) and strain discontinuity (representing heterogeneous strain field); as shown previously for truss-bar structures.²¹

The outline of the paper is as follows. In Section 2, we present the main ingredients of the fracture model for geometrically exact beam, with kinematics that can handle failure modes in softening in terms of 'discontinuity' or 'jump' in the displacement field or the rotational field, depending upon the activated failure mode. In Section 3, we provide a detailed development of non-local constitutive model of finite deformation plasticity in localized failure. The details of FEM implementation based upon the embedded discontinuity approach are presented in Section 4, along with the operator split solution method. The results of several illustrative numerical simulations are given in Section 5, followed by concluding remarks in Section 6.

2 | FRACTURE OF GEOMETRICALLY EXACT REISSNER BEAM

We present in this section the two-dimensional Reissner³ beam formulation generalized to large elasto-plastic strains. The kinematics equations in the framework of large displacements employs a rotated strain measure. The linearization of these strain measures allows us to recover the infinitesimal strains for the Timoshenko beam.¹⁷ The elasto-plastic constitutive

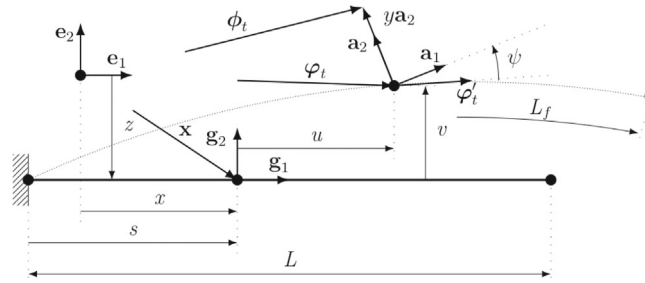


FIGURE 1 Beam kinematics: Initial configuration (thick solid line) and deformed configuration (thin dashed line) with large displacements u and v of beam axis and large rotation ψ of beam cross-section.

equations operate on the finite strains to provide the corresponding stress resultants in agreement with the chosen yield criterion introducing the interaction between axial force, shear force and bending moment. These constitutive equations can also be expressed in rate form.⁸

The solution method is based on the finite element method,⁷ using the geometrically exact beam finite elements with embedded discontinuity, which is needed for modeling softening response phase resulting with localized failure and fracture. The fracture point is not prescribed, but it develops in agreement with the chosen plasticity criteria. We note that this is a more general choice than the one²² dealing with the failure process in the connections, where fracture points coincide with connections. For simplicity, we model separately the failure modes in bending, in shearing or in axial extension. This requires a multiplicative decomposition of the deformation gradient into regular and singular parts, which corresponds to the additive decomposition of the displacement gradient.²³ For such a case, the weak form of equilibrium equations is placed in the framework of incompatible modes,²⁰ which allows us to handle the embedded discontinuity computation at the element level.

2.1 | Kinematics at localized failure for geometrically exact beam

The initial configuration of the geometrically exact beam with length L is described by its neutral axis position s and corresponding cross-section A . The beam volume is generated by sweeping the cross-section A along beam domain $s \in [0, L]$. With no loss of generality, we present the developments for an initially straight beam aligned with x axis; see Figure 1. We can thus simplify the developments presented in References 17,24 for the curvilinear beam axis[†], and use simple parameterization with $\mathbf{g}_i \equiv \mathbf{e}_i$, $s \equiv x$ and $\zeta \equiv y$. Let the beam domain Ω be an open bounded set with a piece-wise smooth boundary such that $\partial\Omega = \partial\Omega_u \cup \partial\Omega_\sigma$ and $\emptyset = \partial\Omega_u \cap \partial\Omega_\sigma$.

The set of generalized displacements for the shear-flexible Reissner beam can be denoted $\mathbf{a}_t = (u_t, v_t, \psi_t)^T$, $\mathbf{a}_t \in \mathcal{U}$, which can be used to describe the motion of beam axis and cross-section orientation in deformed configuration with respect to change of pseudo-time parameter t . The position vector for any point in deformed configuration $\boldsymbol{\phi}_t \in \mathcal{V}$ can be presented by following transformation $f : \mathcal{U} \subset \mathbb{R}^3 \rightarrow \mathcal{V} \subset \mathbb{R}^2$, which allows to write:

$$\boldsymbol{\phi}_t = \boldsymbol{\phi}_t + y\mathbf{a}_{2,t} = \begin{bmatrix} x + u_t \\ v_t \end{bmatrix} + y \begin{bmatrix} -\sin \psi_t \\ \cos \psi_t \end{bmatrix} \quad (1)$$

where x and y are coordinates in reference configuration, u and v are displacement components in the global coordinate system in the Euclidean space, ζ is the coordinate along the normal to the beam axis in the reference configuration (here $\zeta \equiv y$) and ψ is cross-section rotation. The corresponding form of the deformation gradient $\mathbf{F}_t := \nabla \boldsymbol{\phi}_t$ will contain the contributions from both displacement and rotation fields, where we can write:

$$\mathbf{F}_t = \underbrace{\begin{bmatrix} 1 + \frac{du_t}{dx} & 0 \\ \frac{dv_t}{dx} & 0 \end{bmatrix}}_{\mathbf{I} + \nabla \mathbf{u}_t} + \underbrace{\begin{bmatrix} -y \frac{d\psi_t}{dx} \cos \psi_t & -\sin \psi_t \\ -y \frac{d\psi_t}{dx} \sin \psi_t & \cos \psi_t \end{bmatrix}}_{\mathbf{I} + \nabla \psi_t} \quad (2)$$

The rotation finite strain measures in the elastic regime^{17,24} can be stated in either material description or spatial description, connected by rotation tensor \mathbf{R} , as written in (3) below:

$$\begin{aligned} \Sigma &= \cos \psi \left(\frac{dx}{dx} + \frac{du}{dx} \right) + \sin \psi \left(\frac{dy}{dx} + \frac{dv}{dx} \right) - 1 \\ \Gamma &= -\sin \psi \left(\frac{dx}{dx} + \frac{du}{dx} \right) + \cos \psi \left(\frac{dy}{dx} + \frac{dv}{dx} \right) \\ K &= \frac{d\psi}{dx} \end{aligned} \Rightarrow \begin{bmatrix} \epsilon \\ \gamma \end{bmatrix} = \mathbf{R} \begin{bmatrix} \Sigma \\ \Gamma \end{bmatrix} \quad \kappa = K \quad (3)$$

In plastic regime, we have to account for irreversible plastic deformation.^{7,25} This requires describing precisely the loading program with pseudo-time parameter t and obtaining the corresponding evolution of internal variables for plasticity through their rate equations.

We need a modified form of the deformation gradient to describe the softening phenomena that reduce the size of the plastic zone, leading to localized plastic failure and fracture. This implies a stress decrease for increasing deformation, with the stress reduced to zero at fracture. In agreement with Griffith,¹⁴ the fracture modes in axial, shear and bending are represented respectively by jumps in displacement components u, v and in rotation ψ , which splits any field into a regular part ($\bar{\bullet}$) (defined everywhere) and an enhanced part ($\bar{\bullet}$) (which occurs at fracture point \bar{x}). Namely, we can write:

$$\begin{aligned} u(x, t) &= \bar{u}(x, t) + H_{\bar{x}}(x) \bar{\bar{u}}(t) \\ v(x, t) &= \bar{v}(x, t) + H_{\bar{x}}(x) \bar{\bar{v}}(t) \\ \psi(x, t) &= \bar{\psi}(x, t) + H_{\bar{x}}(x) \bar{\bar{\psi}}(t) \end{aligned} \quad ; \quad H_{\bar{x}}(x) = \begin{cases} 0, & x < \bar{x} \\ 1, & x \geq \bar{x} \end{cases} \quad (4)$$

where we represented the jump with the Heaviside function $H_{\bar{x}}$ that captures the corresponding displacement or rotation discontinuity due to fracture. The derivative computations can be written introducing the Dirac delta function²⁶ $\delta_{\bar{x}}(x)$ resulting in the additive decomposition of displacements and rotation gradients as:

$$\begin{aligned} \frac{\partial u(x, t)}{\partial x} &= \frac{\partial \bar{u}(x, t)}{\partial x} + \delta_{\bar{x}}(x) \bar{\bar{u}}(t) \\ \frac{\partial v(x, t)}{\partial x} &= \frac{\partial \bar{v}(x, t)}{\partial x} + \delta_{\bar{x}}(x) \bar{\bar{v}}(t) \\ \frac{\partial \psi(x, t)}{\partial x} &= \frac{\partial \bar{\psi}(x, t)}{\partial x} + \delta_{\bar{x}}(x) \bar{\bar{\psi}}(t) \end{aligned} \quad ; \quad \delta_{\bar{x}}(x) = \begin{cases} \infty, & x = \bar{x} \\ 1, & x \neq \bar{x} \end{cases} \quad (5)$$

In the finite deformation framework,¹⁷ such an additive split of displacement/rotation gradient in (4) corresponds to the multiplicative decomposition of deformation gradient for both contributions from displacements and rotation fields:

$$\mathbf{F} = \underbrace{[\mathbf{I} + \nabla \bar{\mathbf{u}}]}_{\bar{\mathbf{F}}_u} \underbrace{[\mathbf{I} + \delta_{\bar{x}}(\mathbf{I} + \nabla \bar{\mathbf{u}})^{-1} \nabla \bar{\bar{\mathbf{u}}}]_{\bar{\bar{\mathbf{F}}}_u}}_{\bar{\bar{\mathbf{F}}}_u} + \underbrace{[\mathbf{I} + \nabla \bar{\psi}]}_{\bar{\mathbf{F}}_\psi} \underbrace{[\mathbf{I} + \delta_{\bar{x}}(\mathbf{I} + \nabla \bar{\psi})^{-1} \nabla \bar{\bar{\psi}}]}_{\bar{\bar{\mathbf{F}}}_\psi} \quad (6)$$

The final form of kinematics equations should fit within the stress resultant formulation, pertaining to a cross-section of the Reissner beam, which remains straight. Thus, in the polar decomposition of the deformation gradient we further use only the regular part of rotation $\mathbf{F} = \bar{\mathbf{R}}\mathbf{U}$, resulting in the rotated strain measure \mathbf{H} written as:

$$\mathbf{H} = \mathbf{U} - \mathbf{I} ; \quad \mathbf{U} = \bar{\mathbf{R}}^T \mathbf{F} ; \quad \bar{\mathbf{R}} = \begin{bmatrix} \cos \bar{\psi} & -\sin \bar{\psi} \\ \sin \bar{\psi} & \cos \bar{\psi} \end{bmatrix} \quad (7)$$

where \mathbf{U} is the stretch tensor, \mathbf{I} is the identity tensor and $\bar{\mathbf{R}}$ is the rotation tensor adapted to Reissner's beam kinematics. With the results in (6) and (7), we can obtain the corresponding additive decomposition of the stretch tensor:

$$\mathbf{U} = \underbrace{\bar{\mathbf{R}}^T (\mathbf{I} + \nabla \bar{\mathbf{u}})}_{\bar{\mathbf{U}}_u} + \underbrace{\delta_{\bar{x}} \bar{\mathbf{R}}^T \nabla \bar{\bar{\mathbf{u}}}}_{\delta_{\bar{x}} \bar{\bar{\mathbf{U}}}_u} + \underbrace{\bar{\mathbf{R}}^T (\mathbf{I} + \nabla \bar{\psi})}_{\bar{\mathbf{U}}_\psi} + \underbrace{\delta_{\bar{x}} \bar{\mathbf{R}}^T \nabla \bar{\bar{\psi}}}_{\delta_{\bar{x}} \bar{\bar{\mathbf{U}}}_\psi} \quad (8)$$

where the first part is a regular strain field that can be written explicitly as:

$$\bar{\mathbf{U}}_u = \begin{bmatrix} \left(1 + \frac{d\bar{u}}{dx}\right) \cos \bar{\psi} + \frac{d\bar{v}}{dx} \sin \bar{\psi} & 0 \\ -\left(1 + \frac{d\bar{u}}{dx}\right) \sin \bar{\psi} + \frac{d\bar{v}}{dx} \cos \bar{\psi} & 1 \end{bmatrix}; \quad \bar{\mathbf{U}}_\psi = \begin{bmatrix} -y \frac{d\bar{\psi}}{dx} & 0 \\ 0 & 1 \end{bmatrix} \quad (9)$$

and the second part is an enhanced strain that is needed to properly handle the localized failure phenomena:

$$\delta_{\bar{x}} \bar{\bar{\mathbf{U}}}_u = \begin{bmatrix} (\delta_{\bar{x}} \bar{\bar{u}}) \cos \bar{\psi} + (\delta_{\bar{x}} \bar{\bar{v}}) \sin \bar{\psi} & 0 \\ -(\delta_{\bar{x}} \bar{\bar{u}}) \sin \bar{\psi} + (\delta_{\bar{x}} \bar{\bar{v}}) \cos \bar{\psi} & 0 \end{bmatrix}; \quad \delta_{\bar{x}} \bar{\bar{\mathbf{U}}}_\psi = \begin{bmatrix} -y (\delta_{\bar{x}} \bar{\bar{\psi}}) & 0 \\ 0 & 0 \end{bmatrix} \quad (10)$$

We will further consider $\bar{\mathbf{U}}$ equivalent to elastic stretch and $\delta_{\bar{x}} \bar{\bar{\mathbf{U}}}$ as plastic stretch which quantifies the localized plastic deformation.

2.2 | Strong form and weak form of equilibrium

We note that such a modification that one has to introduce to nonlinear kinematics in order to describe plastic localized failure does not affect the equilibrium equations. The simplest format of strong form equilibrium equation for the geometrically exact beam is given in terms of the stress resultants of the first Piola-Kirchhoff stress tensor \mathbf{P} , which we denote as \mathbf{n} for normal and shear force and with m for bending moment; it is easy to show²⁴ that

$$\begin{aligned} \frac{d\mathbf{n}}{dx} + \mathbf{p} &= 0; \\ \frac{dm}{dx} + \frac{d\varphi}{dx} \times \mathbf{n} + \bar{m} &= 0 \end{aligned} \quad (11)$$

where \mathbf{p} is distributed load and \bar{m} is distributed moment. The strong form of equilibrium equations can also be written in terms of the stress resultants of the Biot stress¹⁷ \mathbf{T} , which can be defined by the pull-back²⁷ of the first Piola-Kirchhoff stress \mathbf{P} with the rotation tensor \mathbf{R} ; we can thus write the Cauchy principle for stress vector⁷ as

$$\mathbf{T}\mathbf{e}_1 = \mathbf{R}^T \mathbf{P}\mathbf{e}_1 \Rightarrow \begin{bmatrix} T^{11} \\ T^{21} \end{bmatrix} = \mathbf{R}^T \begin{bmatrix} P^{11} \\ P^{21} \end{bmatrix} \quad (12)$$

The strong form of equilibrium equations with Biot stress resultants, with N for normal force, V for shear force and M for bending moment, can then be written as

$$\frac{d}{dx} [\mathbf{R}\mathbf{N}] + \mathbf{p} = \mathbf{0}; \quad \mathbf{N} = \begin{bmatrix} N \\ V \end{bmatrix} \quad (13)$$

as the force equilibrium equations and

$$\frac{dM}{dx} - \frac{d\varphi}{dx} \times \mathbf{R}\mathbf{N} + \bar{m} = 0 \quad (14)$$

as the moment equilibrium equation. The strong form of equilibrium Equations (13) and (14) are identical to the equations stated by Reissner.³

We will first seek to transform the virtual work expression from the stress-strain into the stress resultants form. In this derivation, we concentrate only on internal work. In terms of non-symmetric Piola-Kirchhoff stress \mathbf{P} and its energy conjugate strain measure,²⁷ the deformation gradient \mathbf{F} . The virtual work takes the form

$$G(\mathbf{a}, \hat{\mathbf{a}}) := \int_L \int_A \hat{\mathbf{F}} \cdot \mathbf{P} \, dA \, dx - \int_L \hat{\mathbf{a}} \cdot \mathbf{p} \, dx = 0 \quad (15)$$

where $\hat{\mathbf{F}}$ denotes the deformation gradient for the virtual displacement field $\hat{\mathbf{a}}$ and \mathbf{a} are current real displacements. The $\hat{\mathbf{F}}$ can be obtained by taking the directional derivative of the deformation gradient \mathbf{F} given in (16),

$$\hat{\mathbf{F}} = \frac{d}{dt} [\mathbf{F}(\mathbf{a} + t\hat{\mathbf{a}})]|_{t=0} \quad (16)$$

or, in component form, we get

$$\begin{aligned} \hat{F}_1^1 &= \frac{d\hat{u}}{dx} - y \frac{d\hat{\psi}}{dx} \cos \psi + \hat{\psi} y \frac{d\psi}{dx} \sin \psi \\ \hat{F}_1^2 &= \frac{d\hat{v}}{dx} - y \frac{d\hat{\psi}}{dx} \sin \psi - \hat{\psi} y \frac{d\psi}{dx} \cos \psi \\ \hat{F}_2^1 &= -\hat{\psi} \cos \psi ; \hat{F}_2^2 = -\hat{\psi} \sin \psi \end{aligned} \quad (17)$$

By using (17), we can rewrite the component form of the stress divergence term in (15) as

$$\begin{aligned} G^{int}(\mathbf{a}, \hat{\mathbf{a}}) &:= \int_L \int_A (\hat{F}_1^1 P^{11} + \hat{F}_1^2 P^{21} + \hat{F}_2^1 P^{12} + \hat{F}_2^2 P^{22}) dA dx \\ &= \int_L \left[\frac{d\hat{u}}{dx} \int_A P^{11} dA + \frac{d\hat{v}}{dx} \int_A P^{21} dA - \frac{d\hat{\psi}}{dx} \int_A y \begin{bmatrix} \cos \psi \\ \sin \psi \end{bmatrix}^T \begin{bmatrix} P^{11} \\ P^{21} \end{bmatrix} dA \right] dx \\ &\quad + \int_L \left[-\hat{\psi} \frac{d\psi}{dx} \int_A \zeta \begin{bmatrix} -\sin \psi \\ \cos \psi \end{bmatrix}^T \begin{bmatrix} P^{11} \\ P^{21} \end{bmatrix} dA - \hat{\psi} \int_A \begin{bmatrix} \cos \psi \\ \sin \psi \end{bmatrix}^T \begin{bmatrix} P^{12} \\ P^{22} \end{bmatrix} dA \right] dx \end{aligned} \quad (18)$$

As a part of the general relationship between the non-symmetric Piola-Kirchhoff stress \mathbf{P} and the Biot stress \mathbf{T} in (12), we can get

$$\mathbf{P}\mathbf{e}_1 = \mathbf{R}\mathbf{T}\mathbf{e}_1 \Rightarrow \begin{bmatrix} P^{11} \\ P^{21} \end{bmatrix} = \begin{bmatrix} T^{11} \cos \psi - T^{21} \sin \psi \\ T^{11} \sin \psi + T^{21} \cos \psi \end{bmatrix} \quad (19)$$

We can further use the relationship²⁷ between non-symmetric \mathbf{P} and symmetric Piola-Kirchhoff stress \mathbf{S}

$$\mathbf{P} = \mathbf{F}\mathbf{S} \quad (20)$$

and the symmetry of \mathbf{S} enforcing that

$$JS^{12} = JS^{21}; J := \det \mathbf{F} = \left(\frac{dx}{dx} + \frac{du}{dx} \right) \cos \psi + \left(\frac{dy}{dx} + \frac{dv}{dx} \right) \sin \psi - \frac{d\psi}{dx} y T^{21} \quad (21)$$

which can be used to further simplify the internal work expression. Namely, utilizing the relationships in (19) and (21), the internal work in (18) can be rewritten in matrix notation as

$$G^{int}(\mathbf{a}, \hat{\mathbf{a}}) := \int_L \left\langle \mathbf{b}^T(\hat{\mathbf{a}})\boldsymbol{\Lambda} + \hat{\psi} \mathbf{h}^T(\mathbf{a}) \frac{d\boldsymbol{\Lambda}}{d\psi} \right\rangle r dx \quad (22)$$

where we define different arrays for writing the Biot strain variations

$$\mathbf{a} = \begin{bmatrix} u \\ v \\ \psi \end{bmatrix}; \hat{\mathbf{a}} = \begin{bmatrix} \hat{u} \\ \hat{v} \\ \hat{\psi} \end{bmatrix}; \mathbf{b}(\hat{\mathbf{a}}) = \begin{bmatrix} \frac{d\hat{u}}{dx} \\ \frac{d\hat{v}}{dx} \\ \frac{d\hat{\psi}}{dx} \end{bmatrix}; \boldsymbol{\Lambda} = \begin{bmatrix} \cos \psi & \sin \psi & 0 \\ -\sin \psi & \cos \psi & 0 \\ 0 & 0 & 1 \end{bmatrix}; \mathbf{h}(\mathbf{a}) = \begin{bmatrix} \frac{dx}{dx} + \frac{du}{dx} \\ \frac{dy}{dx} + \frac{dv}{dx} \\ \frac{d\psi}{dx} \end{bmatrix} \quad (23)$$

along with the work-conjugate stress resultants of the Biot stress

$$\mathbf{r} = \langle N, V, M \rangle^T; \quad N = \int_A T^{11} dA; \quad V = \int_A T^{21} dA; \quad M = \int_A -yT^{11} dA \quad (24)$$

Combining the final result for the internal work given in (22) with the external work, we recover the virtual work expression in terms of stress resultants written in matrix notation as

$$G(\mathbf{a}, \hat{\mathbf{a}}) := \int_L \left\langle \mathbf{b}^T(\hat{\mathbf{a}})\mathbf{\Lambda} + \hat{\psi} \mathbf{h}^T(\mathbf{a}) \frac{d\mathbf{\Lambda}}{d\psi} \right\rangle \mathbf{r} ds - \int_L \hat{\mathbf{a}}^T \mathbf{p} dx = 0 \quad (25)$$

Remark on elastic constitutive equations in stress resultants

For illustration, we here define the simplest set of linear elastic constitutive equations for finite strain beam as Hooke's law connecting the Reissner strain measures and stress resultants of Biot stress. This choice does not fail in satisfying the strain energy poly-convexity condition, such as the St.Venant-Kirchhoff constitutive model,⁷ and can accommodate large strains. Again, this choice is made only for illustration of final model ingredient, and more representative constitutive model is defined in subsequent section. The chosen constitutive model can be written in matrix notation as

$$\mathbf{r} = \underbrace{\mathbf{C}\mathbf{\Lambda}^T}_{\mathbf{\Sigma}}(\mathbf{h}(\mathbf{a}) - \mathbf{a}_1); \quad \mathbf{r} := \begin{bmatrix} N \\ V \\ M \end{bmatrix}; \quad \mathbf{C} = \text{diag}(EA, GA, EI); \quad \mathbf{\Sigma} := \begin{bmatrix} \Sigma \\ \Gamma \\ K \end{bmatrix} \quad (26)$$

With the simplest set of elastic constitutive equations in (26) the strain energy takes a quadratic form. Hence, the expression for the total energy for a finite strain beam can be written as

$$\Pi(\mathbf{a}) = \int_L \frac{1}{2} \langle \mathbf{h}(\mathbf{a}) - \mathbf{a}_1 \rangle^T \mathbf{\Lambda} \mathbf{C} \mathbf{\Lambda}^T (\mathbf{h}(\mathbf{a}) - \mathbf{a}_1) dx - \int_L \mathbf{a}^T \mathbf{p} dx \quad (27)$$

We note in passing that such a quadratic form is consistent with the virtual work expression in (25) obtained as the directional derivative of the expression for the total energy. We also note that such a quadratic form is consistent with the corresponding one for the geometrically linear theory,¹⁷ which can be confirmed by the consistent linearization at the reference configuration, and making an assumption on shallow beam reference geometry.

3 | NON-LOCAL CONSTITUTIVE MODEL OF FINITE DEFORMATION PLASTICITY IN LOCALIZED FAILURE

With the deformation gradient and corresponding strain measures defined in previous section, we can here construct more general constitutive equations for finite deformation plasticity model for localized failure by using the work-conjugate Biot stress \mathbf{T} .

3.1 | Elastic and plastic hardening regimes

We first note that the elastic regime is already defined with constitutive equations written in (26), with elastic deformation replacing the total deformation. For plastic hardening regime, we can still write the strain energy density potential for any point $x \in [0, L]$ of Reissner's beam with cross-section A ; hence, we can formally write:

$$\int_A \Psi(\mathbf{U}) dA := \int_A \frac{1}{2} \bar{\mathbf{F}} \cdot \mathbf{P} dA \equiv \int_A \frac{1}{2} \bar{\mathbf{U}} \cdot \underbrace{\bar{\mathbf{R}} \mathbf{P}}_{\mathbf{T}} dA \quad (28)$$

but any stress tensor we use (\mathbf{P} or \mathbf{T}) now depends on both elastic and plastic strains. In particular, we can start by using 3D model of the beam domain and use any standard plasticity criteria defined at finite strains for solids that employs

standard multiplicative decomposition of deformation gradient $\mathbf{F} = \mathbf{F}^e \mathbf{F}^p$. For example the Mises criterion defined for large strains⁷ can be written in terms of principal values of the second Piola-Kirchhoff stress $\mathbf{S} = \mathbf{F}^{-1} \mathbf{P}$, which have to be computed by solving the eigenvalue tensor with $\mathbf{C} = \mathbf{F}^T \mathbf{F}$ as the metric tensor; hence, we can write such yield criterion as

$$\Phi(\mathbf{S}, \mathbf{C}) \leq 0 ; \mathbf{S} = \mathbf{U}^{-1} \mathbf{T} \Rightarrow \Phi(\mathbf{T}, \mathbf{C}) \leq 0 \quad (29)$$

For final computations with Reissner's beam model in stress resultant form, we further keep only the non-zero Biot stress components, which are obtained from the corresponding non-zero components of the first Piola-Kirchhoff stress \mathbf{P} . Namely, either can be used to define the stress vector \mathbf{t}_1 acting of the beam cross-section by using the Cauchy principle⁷ according to:

$$\mathbf{t}_1 := \mathbf{T} \mathbf{e}_1 \equiv \bar{\mathbf{R}}^T \mathbf{P} \mathbf{e}_1 \Rightarrow \mathbf{t}_1 = \begin{bmatrix} T^{11} \\ T^{21} \end{bmatrix} = \bar{\mathbf{R}}^T \begin{bmatrix} P^{11} \\ P^{21} \end{bmatrix} \quad (30)$$

For plastic hardening regime, we must finally define the yield criterion in the stress-resultant format. The first possibility is to use analytical result obtained for a rectangular cross section,⁸ resulting with three special cases of only two stress resultants active resulting with

$$\begin{aligned} \Phi(N, V, 0) &:= (N/N_y)^2 + (V/V_y)^2 - 1 \\ \Phi(N, 0, M) &:= (N/N_y)^2 + |M/M_y| - 1 \\ \Phi(0, V, M) &:= (V/V_y)^4 + |M/M_y| - 1 \end{aligned} \quad (31)$$

where N_y , V_y and M_y are fully plastic values in the absence of the other two stress resultants. One general form of the yield function which allows recovering the special cases above is suggested⁸ as:

$$\Phi(N, V, M) := |M/M_y| + (N/N_y)^2(1 + (V/V_y)^2) + (V/V_y)^4 - 1 \leq 0 \quad (32)$$

The second possibility is to use homogenisation-like approach, by following previous work² to obtain the corresponding stress resultant form by imposing the stress field on the representative volume element of the Reissner beam in agreement with beam-like distribution of the Biot stress as defined in (24). One such illustration is given in Figure 2 for the simulation obtained by the finite plasticity $F^e F^p$ approach in solids and the corresponding moment-rotation diagram that can be used for training the reduced model of Reissner's beam. The match of the results obtained by a refined model and the Reissner beam model only concern the Quantity-of-Interest, which is chosen as the energy or dissipated energy (as the best choice for the finite element model).

This can produce simplified constitutive response for Reissner's beam as illustrated in Figure 2. Here, the hardening law can be taken simply as linear, or yet exponential to obtain a better fit to experimental results or to 3D solid model to push the stress towards the ultimate value, which will then trigger the softening regime.

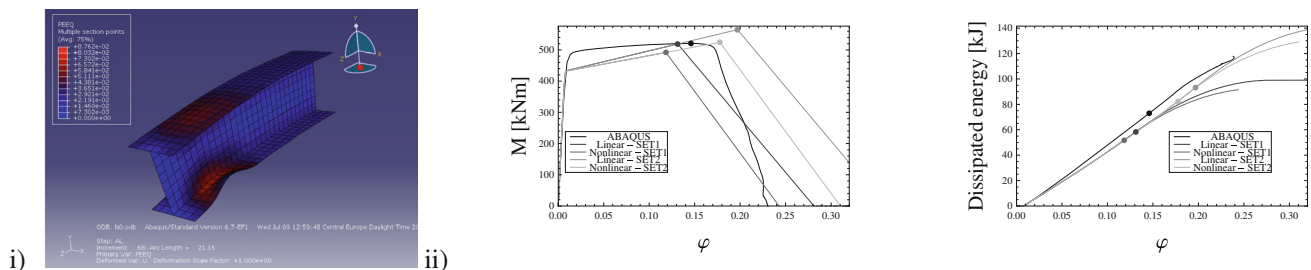


FIGURE 2 Computation on representative volume element for Reissner's beam with a more refined model: (i) Deformed shape and plastic zone obtained by large strain $F^e F^p$ plasticity model for solids; (ii) Corresponding moment-rotation diagram and dissipation that can be used for training the reduced model of Reissner's beam.

3.2 | Plastic softening regime

For plastic softening regime leading to localized plasticity, we have to modify the free-energy potential and introduce two novelties. First, we have to 'regularize' the rotation field by introducing a chosen 'influence' $\tilde{G}(x)$ that can represent the effect of the localized plasticity process at \bar{x} and corresponding energy transfer to the rest of the structure. This can be written as:

$$\mathbf{U}(x, t) = \bar{\mathbf{U}}(x, t) + \tilde{G}(x)\bar{\bar{\mathbf{U}}}(t) + \delta_{\bar{x}}(x)\bar{\bar{\mathbf{U}}}(t) \quad (33)$$

We simplify further development to bending fracture where plastic hinge occurs at point \bar{x} in beam with $\bar{u} = \bar{v} = 0$ and introduce the local support[‡] through influence function that limits the transfer to local region \tilde{L} that surrounds the failure point \bar{x} , which allows us to modify the result in (33) to

$$\mathbf{U}(x, t) = \underbrace{\bar{\mathbf{U}}(x, t) + \tilde{G}(x)\bar{\bar{\mathbf{U}}}^{\psi}(t)}_{\tilde{\mathbf{U}}(x, t)} + \delta_{\bar{x}}(x)\bar{\bar{\mathbf{U}}}^{\psi}(t) \quad (34)$$

Second, the strain energy for localized plasticity in (28) should be split between a regular part for elastic response Ψ^e and a singular part for plastic softening contribution Ξ^p , which can be written as:

$$\Psi(\tilde{\mathbf{U}}, \xi^p) := \underbrace{\frac{1}{2}\tilde{\mathbf{U}}^T \cdot \mathbf{C}\tilde{\mathbf{U}}}_{\Psi^e(\tilde{\mathbf{U}})} + \underbrace{\delta_{\bar{x}}\frac{1}{2}\xi^p\bar{K}\xi^p}_{\Xi^p(\xi^p)}; \quad \forall x \in (\bar{x} - \tilde{L}/2, \bar{x} + \tilde{L}/2) \quad (35)$$

where \mathbf{C} is the elasticity tensor, \bar{K} is the corresponding softening modulus and ξ^p is the equivalent plastic bending strain as an internal variable that describes the plastic flow in softening for localized failure at \bar{x} due to bending moment. This failure mode evolution is governed by the yield criterion that defines a constraint on plastically admissible Biot stress, which can be written in terms of stress-resultant traction at the discontinuity, $t_m = M(\bar{x})$ and stress-like variable q conjugate to an internal variable quantifying softening; we write:

$$\Phi(t_m, q) := [|t_m| - (M_u - q)]_{\bar{x}} \leq 0; \quad q := -\frac{d\Xi^p(\xi^p)}{d\xi^p} = -\bar{K}\xi^p; \quad (36)$$

where M_u is the ultimate value of the bending moment that triggers softening failure. We note that the softening leads to the reduction of elastic domain (with $\bar{K} < 0$ and $\xi^p \geq 0$) until the final failure reducing Reissner's beam bending moment bearing capacity to zero at $\xi_u^p = M_u/|\bar{K}|$.

We next use the second principle of thermodynamics^{7,25} stating that the plastic dissipation is always either positive (in the plastic regime) or zero (in the elastic regime). For softening failure, we need to use a non-local interpretation of the second principle by integrating the dissipation rate over the complete volume ($V = L \times A$) of Reissner's beam, which can be written as:

$$\begin{aligned} 0 &\leq \int_L \int_A \mathcal{D}^p dA dx = \int_L \int_A \left\{ \mathbf{T} \cdot \dot{\mathbf{U}} - \frac{d}{dt} \Psi(\mathbf{U}, \xi_{\bar{x}}^p) \right\} dA dx \\ &= \int_{L-\tilde{L}} \int_A \left\{ \left(\mathbf{T} - \frac{d\Psi^e}{d\bar{\mathbf{U}}} \right) \cdot \dot{\bar{\mathbf{U}}} \right\} dA dx + \left[t_m \frac{\dot{\bar{\psi}}}{\bar{x}} \right]_{\bar{x}} - \int_L \int_A \left\{ \frac{d\Psi^e}{d\bar{\mathbf{U}}} \cdot \dot{\bar{\mathbf{U}}} \right\} dA dx \\ &\quad - \left[\frac{d}{dt} \Xi^p(\xi^p) \right]_{\bar{x}} \end{aligned} \quad (37)$$

where we used the well-known result²⁶ regarding the Dirac delta function to conclude

$$\int_0^L \delta_{\bar{x}}(x) \int_A \left\{ \mathbf{T} \cdot \bar{\bar{\mathbf{U}}}^{\psi} \right\} dA dx = \underbrace{M(\bar{x})}_{t_m} \frac{\dot{\bar{\psi}}}{\bar{x}} \quad (38)$$

In the elastic regime, where the yield function value is negative (with $\Phi(\cdot) < 0$), the internal variable remains frozen (with $\dot{\xi}^p = 0$) and the plastic dissipation rate is equal to zero. Thus, we can obtain from the first term in (37) the set of local constitutive equations for computing the Biot stress (valid at the current value of $\xi^p \equiv \bar{\bar{\psi}}$)

$$\begin{aligned} \mathbf{T} &:= \frac{d\Psi^e}{d\bar{\mathbf{U}}} = \mathbf{C}\bar{\mathbf{U}}; \quad \forall x \in (0, \bar{x} - \bar{L}/2) \cup (\bar{x} + \bar{L}/2, L); \\ \mathbf{T} &:= \frac{d\Psi^e}{d\bar{\mathbf{U}}} = \mathbf{C}\bar{\mathbf{U}}; \quad \forall x \in (\bar{x} - \bar{L}/2, \bar{x} + \bar{L}/2) \end{aligned} \quad (39)$$

In the plastic regime corresponding to zero value of the yield criterion (with $\Phi(\cdot) = 0$), we have to compute the plastic dissipation and flow equations. Here, we assume that the constitutive equations above remain valid, with the internal variable evolution much faster than the change of the state variables. We also enforce the weak form of equilibrium equation within the domain of influence of localized failure to obtain

$$h(\cdot) := t_m \dot{\bar{\psi}} - \int_{\bar{x}-\bar{L}/2}^{\bar{x}+\bar{L}/2} \tilde{G}(x) \underbrace{\int_A \mathbf{T} \cdot \dot{\bar{\mathbf{U}}}^{\psi} dA}_{M(x)\dot{\bar{\psi}}} dx = 0 \quad (40)$$

Thus, with (36) and (37), we can obtain that the only contribution to plastic dissipation rate is reduced to discontinuity

$$0 < D_{\bar{x}}^p = [q_s^{\dot{\xi}^p}]_{\bar{x}} \quad (41)$$

Having defined localized plastic dissipation, we can obtain the remaining results by using the principle of maximum plastic dissipation^{7,18} stating that among all plastically admissible values of stress one must pick the one maximizing plastic dissipation:

$$q = \min_{\Phi(t_m, q)=0} \left[-D_{\bar{x}}^p(q^*) \right]_{\bar{x}} \quad (42)$$

The principle of maximum plastic dissipation applied to the case where only discontinuity remains active can be written by introducing the localized Lagrange multiplier in the form:

$$\dot{\gamma}(x, t) = \delta_{\bar{x}}(x) \dot{\gamma}_{\bar{x}}(t) \quad (43)$$

The constrained minimization in (42) can be replaced with unconstrained optimization, by introducing the corresponding plastic Lagrangian

$$\max_{\dot{\gamma}} \min_{\forall (t_m, q)} \mathcal{L}^p(q, \dot{\gamma}_{\bar{x}}); \quad \mathcal{L}^p(\cdot) := -D_{\bar{x}}^p(\cdot) + \int_0^L \dot{\gamma} \Phi(\cdot) \quad (44)$$

but the localized Lagrange multiplier in (43) further restricts the constraint to discontinuity according to:

$$\mathcal{L}^p(\cdot) := [-q \dot{\xi}^p + \dot{\gamma}_{\bar{x}} \Phi(\cdot)]_{\bar{x}} \quad (45)$$

The Kuhn-Tucker optimality conditions then reduces to rate equation for softening internal variable

$$\frac{\partial \mathcal{L}^p}{\partial q} = 0 \Rightarrow \dot{\xi}^p = \dot{\gamma}_{\bar{x}} \underbrace{\frac{\partial \Phi}{\partial q}}_{=1} \quad (46)$$

accompanied by loading-unloading conditions, if one includes both elastic and plastic process

$$\frac{\partial \mathcal{L}^p}{\partial \dot{\gamma}_{\bar{x}}} = 0 \Rightarrow \Phi(\cdot) \leq 0; \dot{\gamma}_{\bar{x}} \geq 0; \dot{\gamma}_{\bar{x}} \Phi(\cdot) = 0 \quad (47)$$

We have thus defined all governing equations to be solved at the local level. In discrete approximation, the solution of local governing equations is computed by time integration scheme at the Gauss point of the finite element undergoing localized failure, in order to enforce the local constraint of plastic admissibility of stress and to compute the evolution of the internal variable corresponding to rotation discontinuity.

We note that softening modulus $\bar{K} < 0$ is not easy to identify, and we rather use fracture energy G_f as the model parameter for softening plasticity. We can compute the fracture energy G_f in a pure bending test (with $M(x, \bar{t}) = cst.$), as the equivalent energy of external forces applied to a Reissner's beam with constitutive behavior of softening plasticity that is needed to reduce the effective stress-resultant to zero, with

$$M_u - q_u = M_u - \underbrace{|\bar{K}| \overbrace{M_u/|\bar{K}|}^{\xi_u^p}}_{q_u} = 0 \quad (48)$$

This computation is performed by integrating the total dissipation as defined from the Clausius-Duhem inequality in (37) for a given proportional loading program, which starts with zero applied traction at time t_0 , peaks to a maximum value at time t_u and goes down to zero value again as the result of softening at time t_f ; we can thus write:

$$\underbrace{\int_{t_u}^{t_f} \left[\int_L M_u \dot{\gamma} dx \right] dt}_{M_u \xi_u^p} = \underbrace{\int_{t_0}^{t_f} \int_L M \dot{\kappa} dx dt}_{G_f} - \underbrace{\int_{t_u}^{t_f} \frac{d}{dt} \int_L \delta_{\bar{x}} \Xi(\xi^p) dx dt}_{-(1/2) \xi_u^p |\bar{K}| \xi_u^p} \quad (49)$$

where we took into account that $\int_{t_0}^{t_f} \frac{d}{dt} \int_V \Psi^e(\bar{\mathbf{U}}) dx dt = 0$. For the softening plasticity model with linear softening modulus $\bar{K} = cst. < 0$, the zero value of the effective stress corresponds to the maximum value of the rotation discontinuity $\xi_u^p = M_u/|\bar{K}|$; from (49), we can further obtain that:

$$M_u \frac{M_u}{|\bar{K}|} = G_f + \frac{1}{2} \frac{M_u}{|\bar{K}|} |\bar{K}| \frac{M_u}{|\bar{K}|} \Rightarrow G_f = \frac{1}{2} \frac{M_u^2}{|\bar{K}|} \Leftrightarrow |\bar{K}| = \frac{1}{2} \frac{M_u^2}{G_f} \quad (50)$$

The last result shows that the fracture energy is equal to the area of the triangle below the softening part of the response, which starts at the peak value of resistance (where $M = M_u$) and which ends at the final failure state with zero effective stress (where $M = 0$). It is also possible to obtain the corresponding expression for G_f with any other form of post-peak softening response.⁷

4 | STRESS RESULTANT PLASTICITY DISCRETE APPROXIMATION AND SOLUTION PROCEDURE

In this section we provide the reduced model in stress resultant form of the proposed localized plasticity for Reissner's beam, its discrete approximation and an outline of the computational procedure.

4.1 | Stress resultant format of localized plasticity for Reissner's beam

In order to recast the proposed plasticity model in stress resultant form for the Reissner³ beam, we impose the kinematic constraint on a rigid cross-section moved by large rotation, which results with only two non-zero strain components of the rotated strain tensor $H_{11} = \Sigma - yK$ and $H_{21} = \Gamma$. For finite deformation plasticity with softening in beam bending, these strain measures are regularized by influence function \tilde{G} , which can be written as

$$\begin{aligned}
\tilde{\Sigma} &= \underbrace{\left(1 + \frac{d\bar{u}}{dx}\right) \cos \bar{\psi} + \frac{d\bar{v}}{dx} \sin \bar{\psi}}_{\bar{\Sigma}} - 1 \\
\tilde{\Gamma} &= - \underbrace{\left(1 + \frac{d\bar{u}}{dx}\right) \sin \bar{\psi} + \frac{d\bar{v}}{dx} \cos \bar{\psi}}_{\bar{\Gamma}} \\
\tilde{K} &= \underbrace{\frac{d\bar{\psi}}{dx}}_{\bar{K}} + \underbrace{\frac{d\bar{\psi}}{dx}}_{\bar{K}} \tilde{G}
\end{aligned} \tag{51}$$

The result in (51) that can be rewritten in matrix notation:

$$\tilde{\Sigma} = \Lambda^T (h(\bar{a}) - a_1) + \tilde{G} \bar{K} e_3 \tag{52}$$

where

$$\begin{aligned}
\tilde{\Sigma} &= \begin{pmatrix} \tilde{\Sigma} \\ \tilde{\Gamma} \\ \tilde{K} \end{pmatrix}; \Lambda = \begin{bmatrix} \cos \bar{\psi} & -\sin \bar{\psi} & 0 \\ \sin \bar{\psi} & \cos \bar{\psi} & 0 \\ 0 & 0 & 1 \end{bmatrix}; a_1 = \Lambda e_1 \\
\bar{a} &= \begin{pmatrix} \bar{u} \\ \bar{v} \\ \bar{\psi} \end{pmatrix}; b(\hat{a}) = \begin{pmatrix} \frac{d\hat{u}}{dx} \\ \frac{d\hat{v}}{dx} \\ \frac{d\hat{\psi}}{dx} \end{pmatrix}; h(\bar{a}) = \begin{pmatrix} 1 + \frac{d\bar{u}}{dx} \\ \frac{d\bar{v}}{dx} \\ \frac{d\bar{\psi}}{dx} \end{pmatrix}; e_1 = \begin{pmatrix} 1 \\ 0 \\ 0 \end{pmatrix}; e_3 = \begin{pmatrix} 0 \\ 0 \\ 1 \end{pmatrix}
\end{aligned} \tag{53}$$

By using further the same matrix notation for the virtual strains (denoted with superposed (\hat{a})), we can write the weak form of equilibrium equations in stress resultants with:

$$\begin{aligned}
G_{\bar{a}}(\bar{a}, \bar{\psi}; \hat{a}) &:= \int_L \left(b^T(\hat{a}) \Lambda + \hat{\psi} h^T(\bar{a}) \frac{d\Lambda}{d\psi} \right) r \, dx - \int_L \hat{a}^T p^{\text{ext}} \, dx = 0 \\
G_{\bar{\psi}}^e(\bar{a}, \bar{\psi}; \hat{\psi}) &:= \hat{\psi}^T t_m - \int_{L^e} \hat{\psi} \tilde{G}^e M \, dx = 0; \forall e \text{ with } \Phi = 0
\end{aligned} \tag{54}$$

where virtual displacement and rotation field derivatives for the regular part are written in (53). In (54), N , V and M denote stress resultants expressed in terms of the Biot stress, which can be gathered in the vector of internal forces and written in matrix notation:

$$r = (N, V, M)^T; N = \int_A T^{11} dA; V = \int_A T^{21} dA; M = - \int_A y T^{11} dA \tag{55}$$

If the elastic regime, the internal forces are computed from the current values of strain measures (at frozen jump) by multiplying them with Reissner's beam constitutive matrix

$$r = C \tilde{\Sigma}; C = \text{diag}(EA, GA, EI) \tag{56}$$

where EA , GA and EI are respectively elastic stiffness of the beam cross-section for axial force, shear force and bending moment.

In the opposite case for plastic regime, one first has to carry out the local (element-wise) computation of plastic flow and converge at the local level to provide the plastically admissible value of the stress that satisfies $\Phi(\cdot) = 0$. Subsequently, we keep the current values of discontinuity parameters frozen and then carry out one sweep of iterative procedure

at the global (structure) level. For Newton's iteration, we need to carry out consistent linearization to obtain the tangent operators that provide a quadratic convergence rate⁸. Thus, the consistent linearization of the weak form in (54)₁ results with:

$$\begin{aligned} L[G_{\bar{a}}(\cdot)] &= G_{\bar{a}}(\bar{a}, \bar{\psi}; \hat{a}) + \frac{d}{dt} \left[G_{\bar{a}}(\bar{a} + t\Delta\bar{a}, \bar{\psi} + t\Delta\bar{\psi}; \hat{a}) \right] \Big|_{t=0} \\ &= G_{\bar{a}}(\cdot) + \int_L \left(\mathbf{b}(\hat{a}) \quad \hat{\psi} \right) [D_m^K + D_g^K] \begin{pmatrix} \mathbf{b}(\Delta\bar{a}) \\ \Delta\bar{\psi} \end{pmatrix} dx \\ &\quad + \int_L \left(\mathbf{b}^T(\hat{a})\Lambda + \hat{\psi}h^T(\bar{a})\frac{d\Lambda}{d\psi} \right) \text{Ce}_3 \tilde{G} \Delta\bar{\psi} dx = 0 \end{aligned} \quad (57)$$

where D_m^K and D_g^K are defined in (58) below

$$D_m^K = \begin{bmatrix} \Lambda \\ h^T(\bar{a})\frac{d\Lambda}{d\psi} \end{bmatrix} C \left[\Lambda^T \quad \frac{d\Lambda^T}{d\psi} h(\bar{a}) \right]; D_g^K = \begin{bmatrix} 0 & \frac{d\Lambda}{d\psi} r \\ r^T \frac{d\Lambda^T}{d\psi} & h^T(\bar{a})\frac{d^2\Lambda}{d\psi^2} r \end{bmatrix} \quad (58)$$

4.2 | Discrete approximation by embedded discontinuity finite elements

The numerical implementation of the softening plasticity model with displacement discontinuity can nicely fit within the framework of the incompatible mode method.²⁰ The main advantage of the incompatible mode method in this context is its ability to handle the plastic strain computation locally (element-wise), which ensure the computational efficiency by using the operator split further described in this section. We illustrate the pertinent details of numerical implementation for the simplest finite element model using a 2-node isoparametric Reissner's beam element⁴. The rotation discontinuity is represented with an additional parameter α^e , which can further be treated in the same manner as the incompatible mode parameter.²⁰ However, we can choose the element-wise approximation of the influence function such that the rotation values at the element nodes need not be modified; thus, we set:

$$\begin{aligned} x(\xi)|_{\Omega^e} &= \sum_{a=1}^2 N_a(\xi)x_a; \quad N_a(\xi) = \frac{1}{2}(1 + \xi_a\xi); \\ u^h(x, t)|_{\Omega^e} &= \sum_{a=1}^2 N_a(x)d_{a,1}(t); \\ v^h(\xi, t)|_{\Omega^e} &= \sum_{a=1}^2 N_a(\xi)d_{a,2}(t); \\ \psi^h(\xi, t)|_{\Omega^e} &= \sum_{a=1}^2 N_a(\xi)d_{a,3}(t) + M^e(\xi)\alpha^e(t); \\ M^e(\xi) &= \begin{cases} -\frac{1}{2}(1 + \xi), & \text{si } \xi \in [-1, 0] \\ \frac{1}{2}(1 - \xi), & \text{si } \xi \in [0, 1] \end{cases} \end{aligned} \quad (59)$$

The proposed interpolation will place the rotation discontinuity in the center of this element at the Gauss point. The corresponding derivative approximations define the bending strain measure, which can be written:

$$\begin{aligned} \frac{d\psi^h(x, t)}{dx} \Big|_{L^e} &= \sum_{a=1}^2 \underbrace{B_a(x)}_{\frac{dN_a}{dx}} d_{a,3}(t) + \underbrace{G^e(x)}_{\frac{dM}{dx}} \alpha^e(t); \quad B_a(\xi) = \frac{(-1)^a}{L^e}; \\ G^e(x) &= \tilde{G}^e(x) + \delta_0(x); \quad \tilde{G}^e(x) = -\frac{dN_2(x)}{dx}; \quad \delta_0(x) := \begin{cases} 0, & \xi \neq 0 \\ \infty, & \xi = 0 \end{cases} \end{aligned} \quad (60)$$

where δ_0 is the Dirac function centered within the element. In order to ensure the method convergence in the spirit of the patch test, we will make sure that the incompatible mode variation remains orthogonal to the constant moment in each element; such a work-conjugate couple should thus satisfy:

$$\int_{L^e} G^e dx = 0 \Leftrightarrow \int_{L^e} \underbrace{-\frac{1}{L^e}}_{\tilde{G}^e} dx = - \int_{L^e} \delta_0 dx \quad (61)$$

For the present 1D case, with displacement discontinuity placed in the center of the element, the patch test condition in (61) is automatically satisfied leaving G^e intact. We can thus keep exactly the same approximation for the virtual strain field as the one used for real strains

$$\left. \frac{d\hat{\psi}^h(x, t)}{dx} \right|_{\Omega^e} = \sum_{a=1}^2 \underbrace{B_a(x)}_{\frac{dN_a}{dx}} \hat{d}_{a,3}(t) + \underbrace{G^e(x)}_{\frac{dM}{dx}} \hat{\alpha}^e(t) \quad (62)$$

Both of these approximations are constructed with a single Gauss point^{7,28} ($n_{int} = 1$) placed at the center of the element with a weighting factor equal to 2. Such approximation gives the constant values for stress resultant $r := (N^h, V, {}^hM^h)^T$, and can be written in component form as:

$$\begin{aligned} N^h(0, t) &= EA \tilde{\Sigma}^h(0, t) \\ V^h(0, t) &= GA \tilde{\Gamma}^h(0, t) \\ M^h(0, t) &= EI \left[\sum_{a=1}^2 B_a(0) \psi_a(t) + \tilde{G}^e(0) \alpha^e(t) \right] \end{aligned} \quad (63)$$

With these results in hand, we can construct the discrete approximation for the residual vector for a 2-node Reissner's beam element, first with the standard part of the element's internal force

$$\hat{d}^T f^{int,e} = \sum_{l=1}^{n_{int}=1} \left\{ \underbrace{\left\langle b^T(\hat{a}^h) \Lambda^h + \hat{\psi} h^T(a^h) \frac{d\Lambda^h}{d\psi} \right\rangle_{r^h}}_{\hat{d}^T \tilde{B}^T} \right\} \Bigg|_{\xi=0} \underbrace{j(0)}_{L/2} \underbrace{w}_2 \quad (64)$$

and then for the extra terms for the element in which plastic localized failure occurs

$$\hat{\alpha}^h h^e = \hat{\alpha}^h t_m + \hat{\alpha}^h \sum_{l=1}^{n_{int}=1} \{ \tilde{G}^e M^h \} \Big|_{\xi=0} \underbrace{j(0)}_{L/2} \underbrace{w}_2 \quad (65)$$

The bending moment approximation can be obtained from the regular part of the real curvature in (60), with no contribution from the singular part representing the localized plastic curvature; we can thus write:

$$M^h(x, t)|_{L^e} = EI \left(\sum_{a=1}^2 B_a(x) d_{a,3}(t) + \tilde{G}^e(x) \alpha^e(t) \right) \quad (66)$$

By exploiting the approximations for virtual strains and stress, defined in (62) and (66) respectively, the weak form of equilibrium equations can be recast in the format typical of the incompatible mode method:

$$\begin{aligned} \mathbb{A} n_{elem} e = 1 \quad (f^{int,e} - f^{ext,e}) = 0; \quad f^{int,e} &= \int_{L^e} \tilde{B}^{e,T} r(d, \alpha^e) dx \\ h^e = 0 \quad \forall e \in [1, n_{elem}]; \quad h^e &= \int_{L^e} \tilde{G}^{e,T} M(d, \alpha^e) dx + t_m(\alpha) \end{aligned} \quad (67)$$

where $t_m = M|_{\bar{x}}$ is the bending traction acting at the discontinuity. This traction enters the corresponding plasticity criterion $\Phi(t_m, q) = 0$, which requires to obtain the plastic strain and the value of parameter α^e :

$$\Phi(t_m, q) := |t_m| - (M_u - q(\alpha^e)) \leq 0 \quad (68)$$

where q is the variable defining the current plasticity threshold depending upon the rotation discontinuity.

We solve this problem by using the operator split solution procedure for finding the solution to equations in (67) and (68). Namely, we treat separately the local phase from the global phase of computation. We first solve the local phase (defined in (68)) for the given total displacement field and then the global phase (defined in (67)) for the corresponding localized plastic flow. One rather subtle point concerns the role of parameter α^e , which is modified in both local and global phase of computations. Further details of operator split procedure are described in the Appendix.

5 | ILLUSTRATIVE NUMERICAL EXAMPLES

Several numerical examples are presented in this section to illustrate an excellent performance of the proposed finite element formulation. All numerical computations are performed with a research version of the computer program FEAP.^{28,29}

5.1 | Straight cantilever in pure bending–Test result for mesh invariance

In this example, we present different stages of behavior for a geometrically exact beam in pure bending, starting from elastic, followed by a plastic hardening response and eventually by plastic softening response once the ultimate beam resistance is reached. The chosen structure is an initially straight cantilever beam of length $L = 1\text{m}$ (see Figure 3), which is submitted to pure bending load. The simulation is performed by imposed free-end rotation, which allows us to ensure computational robustness and enforce stability in the softening response phase.

The chosen geometric properties of the beam cross-section correspond to standard hot rolled profile IPE 200 and material properties take values for steel class S235 (see Figure 3). More precisely, the chosen properties of the cantilever are: Young's modulus: $E = 2 \cdot 10^5\text{MP}$; hardening modulus: $K = 0.05E$; moment of inertia: $I = 1940 \cdot 10^{-8}\text{m}^4$; area of the cross-section: $A = 28.5 \cdot 10^{-4}\text{m}^2$; yield bending moment: $M_y = 31000\text{Nm}$; ultimate bending moment: $M_u = 38000\text{Nm}$ and fracture energy $G_f = 5500\text{Nm}$.

We use this example where the bending moment remains constant along the beam to illustrate the computed results invariance for different number of elements. More, precisely the results are obtained with the mesh of the initially straight cantilever beam elements by using either 2, 4 or 8 elements. Each analysis is performed under imposed end rotation $\psi = \pi$ and the corresponding bending moment is obtained as a reaction.

The first analysis concerns the elastic beam behavior, obtained with the yield and ultimate moments considered infinite. In Figure 4 we present the computed deformed shape with the finest mesh of 8 beam elements, which places the nodes on the half-circle, which is the exact deformed shape obtained for the elastic case. The computed moment-rotation diagram is linear (see Figure 4), matching the analytic solution for elastic case with the highest value of the reaction moment corresponding to the maximum value of imposed rotation $M := EI\pi/L = 12.189 \cdot 10^6\text{Nm}$.

In the second analysis, we assume that the beam has an elasto-plastic behavior with linear hardening, by assuming that the ultimate moment takes an infinite value. We again obtain the deformed shape as a half-circle for imposed free-end rotation equal to π with the finite element nodes placed along the beam deformed axis (see Figure 5). The corresponding

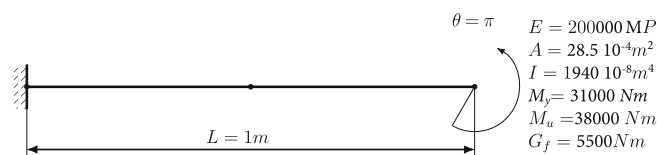


FIGURE 3 Straight cantilever beam with chosen cross-section IPE and steel material S235.

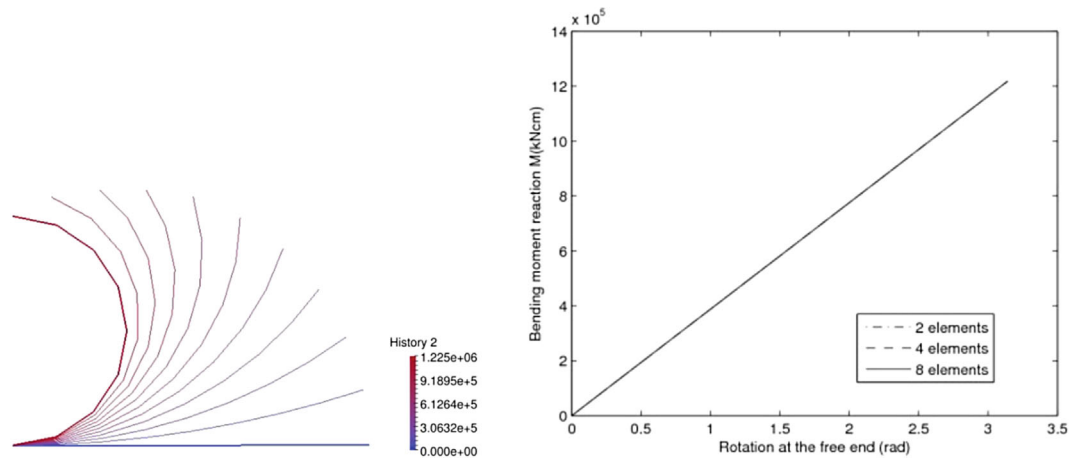


FIGURE 4 Cantilever beam plastic failure with constitutive model accounting for only elastic response: (left) Deformed shapes, (right) force-displacement diagram.

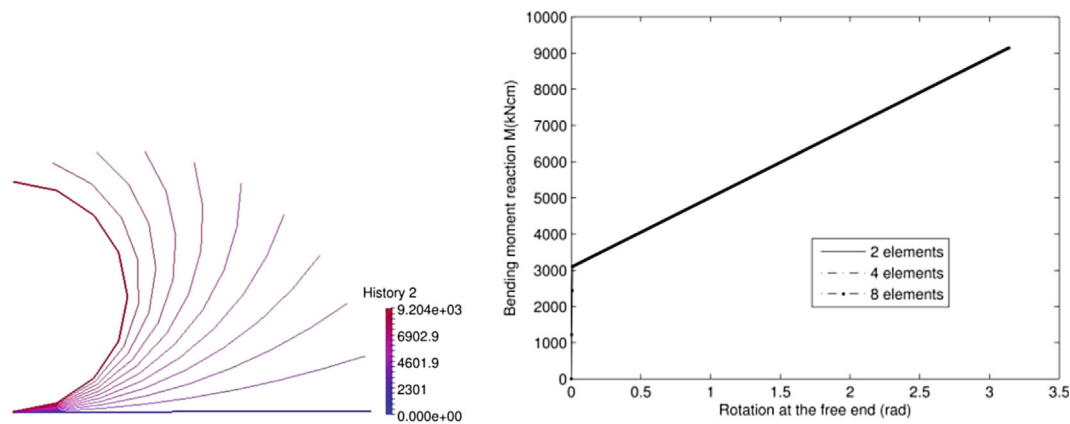


FIGURE 5 Cantilever beam plastic failure with constitutive model accounting for only hardening response: (left) Deformed shapes, (right) force-displacement diagram.

value of the end moment is increasing toward the maximum value computed as $M = M_y + EK(\pi - M_y/EI)/(E + K)L = 9.145 \cdot 10^4 Nm$. The moment-rotation diagram is now bilinear, with marked difference of stiffness between elastic phase and plastic hardening phase (see Figure 5).

The final analysis represents the elasto-plastic response that first goes into a hardening phase until the ultimate moment M_u , followed by subsequent plastic softening. In the plastic softening response phase, which is reducing the beam bearing capacity for bending moment down to zero, the plastic deformation remains localized. More precisely, the fracture is localized in the middle of the cantilever, where one element is weakened (see Figure 6) and the corresponding deformed shape corresponds to the creation of the plastic hinge, while the rest of the beam gets unloaded with residual smooth plastic deformation. The computed moment-rotation diagram represents correctly three different response phases, with the elastic phase followed by plastic hardening and then by plastic softening. It is important that the computed results again remain the same for any number of beam elements, 2, 4 or 8 (see Figure 6). This confirms the mesh objectivity of the proposed formulation.

5.2 | Push-over analysis of a symmetric frame until complete failure

In this example, we present the results of a push-over analysis of a symmetric steel frame. The frame geometry is given in Figure 7. The material properties for all beam elements modelling the columns are equal: Young's

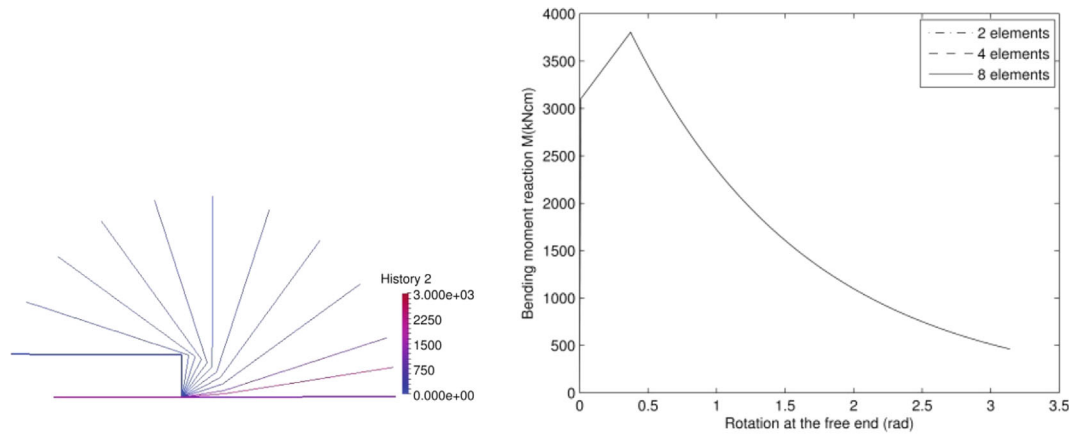
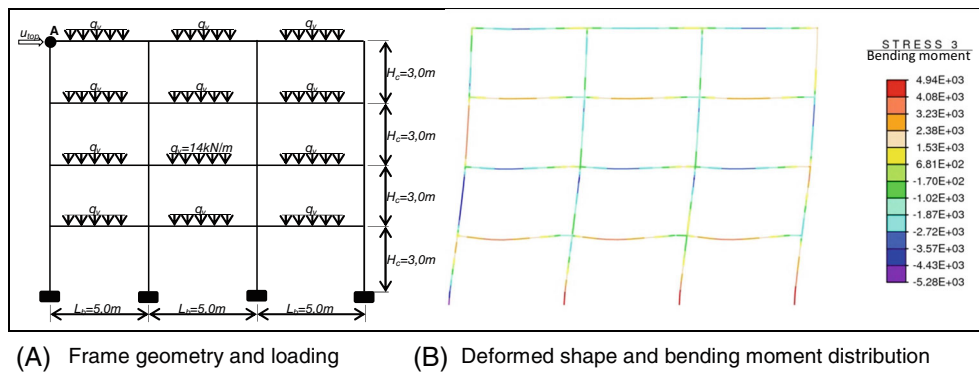


FIGURE 6 Cantilever beam plastic failure with constitutive model that can account for both hardening and softening response phase: (left) Deformed shapes, (right) force-displacement diagram.



(A) Frame geometry and loading **(B)** Deformed shape and bending moment distribution

FIGURE 7 Multi-storey frame: (left) Structure geometry and loading and (right) deformed shape and bending moment distribution.

modulus: $E = 2 \cdot 10^5 \text{ MP}$; hardening modulus: $K = 0.05E$; moment of inertia: $I = 1940 \cdot 10^{-8} \text{ m}^4$; area of the cross-section: $A = 28.5 \cdot 10^{-4} \text{ m}^2$; yield bending moment: $M_y = 31000 \text{ Nm}$; ultimate bending moment: $M_u = 38000 \text{ Nm}$; and fracture energy: $G_{f,M} = 5500 \text{ Nm}$, for all columns. The stiffness of the finite elements modelling the beams is chosen 10% weaker than for those modeling the columns, in order to enforce 'strong-column-weak-beam' frame design and to approximate the behavior of connections in the steel frame structure.

The vertical load was applied to all beam members. This load is kept constant throughout pushover analysis in order to simulate the dead load effect. The lateral loading is applied in terms of an imposed incremental displacement (u_{top}) at the upper corner (point A, see Figure 7). In Figure 7B, we present the deformed configuration of the steel frame and the corresponding distribution of the bending moments. The position of activated plastic hinges in the final stage of structure failure and the computed softening response in terms of the force-displacement diagram are both shown in Figure 8.

5.3 | Nonlinear instability of hinged-clamped circular arch: Elasticity versus elasto-plasticity with softening

This example presents nonlinear instability under the point load of a circular arch whose one end is clamped and the other hinged. The chosen elastic properties for the arch are presented in Figure 9, in agreement with the choice made in previous work³⁰ where the reference value of the critical force is given for the elastic case.

The exact solution for the displacement under the vertical force is obtained³⁰ for Euler's elastica theory (with hypotheses of no shear and no axial strain⁹). To obtain an equivalent numerical result, a penalty-like procedure is used with shear and axial beam stiffness chosen 100 times larger than bending stiffness (see Figure 9). The numerical results are

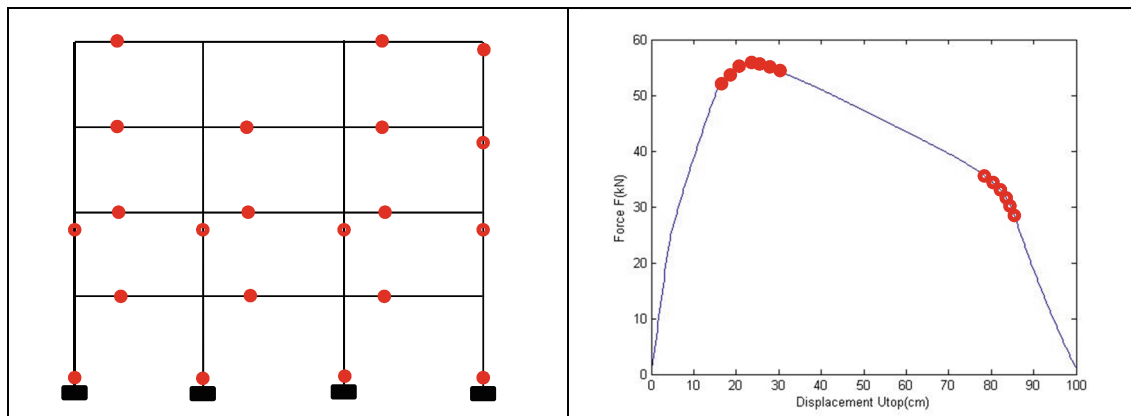


FIGURE 8 Multi-storey frame: (left) Localized hinges at failure and (right) force-displacement diagram until complete failure.

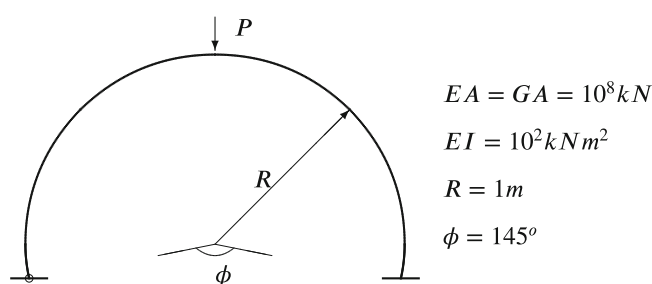


FIGURE 9 Initial configuration of thin circular arch (with right support clamped and left hinged) undergoing nonlinear instability with large pre-critical displacements.

TABLE 1 Critical load for nonlinear instability of circular arch.

Formulation	Critical load (kN)
Present (3-node)	897.5
de Ville de Goyet and Frey ³¹	902.8
Present (2-node)	904
Simo, Hjelmstad and Taylor ⁸	906
Zienkiewicz and Taylor ²⁸	925
Exact ³⁰	897

obtained with 20 quadratic elements and 40 linear elements. All numerical computations are performed with a research version of the computer program *FEAP*.^{28,29} The computed results compare favorably to the results available in the literature with equivalent finite element meshes, especially if an improved discrete approximation is made of the curved geometry with a 3-node geometrically exact beam element; see Table 1. This confirms the interest of using improved representation of beam geometry (such as by IGA¹⁰), in an elastic case where the beam deformed shapes remain smooth.

The value for the critical load is significantly influenced by the large pre-buckling displacements. We refer to Figure 10, where the computed vertical displacement under the force is plotted for different values of force, along with the exact result.³⁰ We can see in Figure 11, that the vertical displacement at the critical equilibrium state is very large, of the order of magnitude of arc radius, and critical force 'flattens' the structure at the critical state.

If we now allow for elastoplastic constitutive behavior with softening for the arch structure, the ultimate load is reduced by the creation of the plastic hinge at the built-in end; see Figure 10. Here, we have chosen the same axial and shear stiffness $EA \equiv GA = 10^8 \text{ kN}$, the bending stiffness $EI = 10^2 \text{ kNm}^2$, the yield moment $M_y = 5 \cdot 10^4 \text{ Nm}$, the

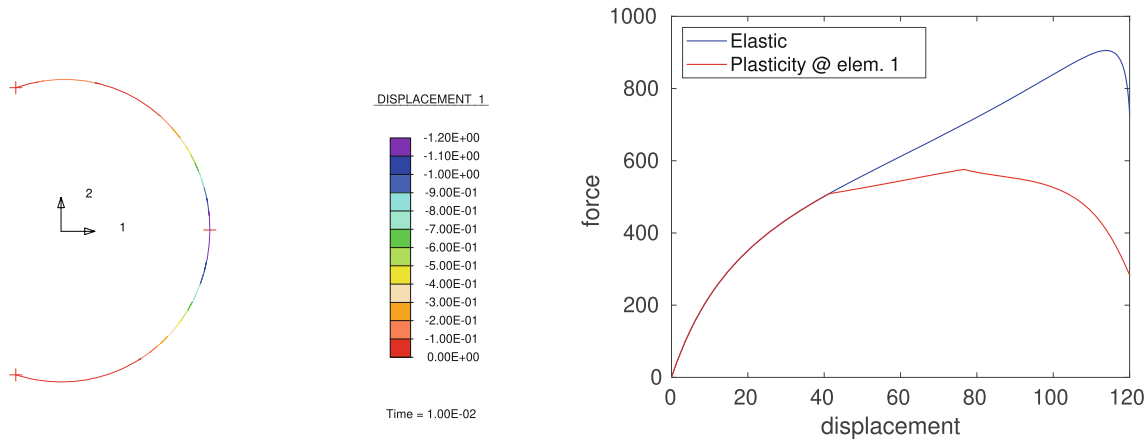


FIGURE 10 Circular arch: (left) Initial configuration; (right) applied load–Deflection curves for elastic and for elastoplastic case with softening.

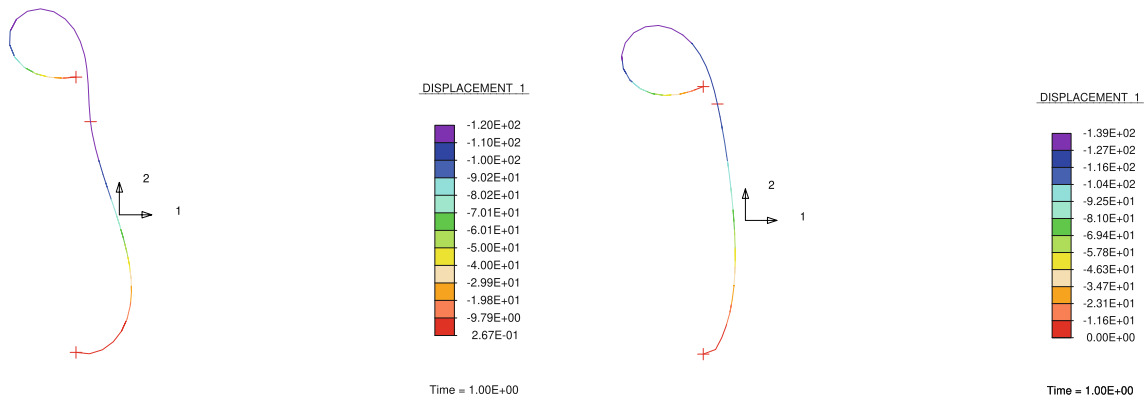


FIGURE 11 Circular arch: Deformed configuration at critical equilibrium state; (left) elastic response (right) plastic response.

hardening stiffness for bending $KI = 0.1EI$, the ultimate moment $M_u = 1 \cdot 10^5 Nm$ and the fracture energy in bending $G_f = 2.5 \cdot 10^5 Nm$. For the chosen values, the plastic hinge is formed at the the built-in end, which modifies the deformed shape; the latter is no longer smooth, featuring the rotation discontinuity in the beam element closest to built-in support; see Figure 11. Thus, the smooth geometry representation (such as IGA) is not likely to be suitable for this case.

We further illustrate the computed results by plotting the diagram bending moment–imposed displacement in the first element next to built-in end (denoted as element 1 in Figure 12). We can also observe that once the plasticity starts, the external energy is no longer stored like in the elastic case, but a part of it is dissipated; see Figure 12.

The condition for finding a critical equilibrium state is still the singularity of the tangent stiffness matrix, with $K\phi_{cr} = 0$, where K is the tangent stiffness and ϕ_{cr} is the critical mode. The tangent stiffness is a (highly) nonlinear function of applied loading, as specified in (58). Here, we here have a typical case of what is called a nonlinear instability problem, where the hypothesis of small pre-buckling displacements will not be justified, which requires special methods for solving such (nonlinear) eigenvalue problem.⁷

5.4 | 3D bending localized failure of flexible blades of wind turbine

In the final example we seek to illustrate the capabilities of our geometrically exact beam model to handle 3D bending failure. In particular, we are able to fully reproduce the typical different deformed configurations of a flexible wind-turbine blade under extreme out-of-plane loads (e.g., wind) leading to localized failure and fracture in bending. We note that such

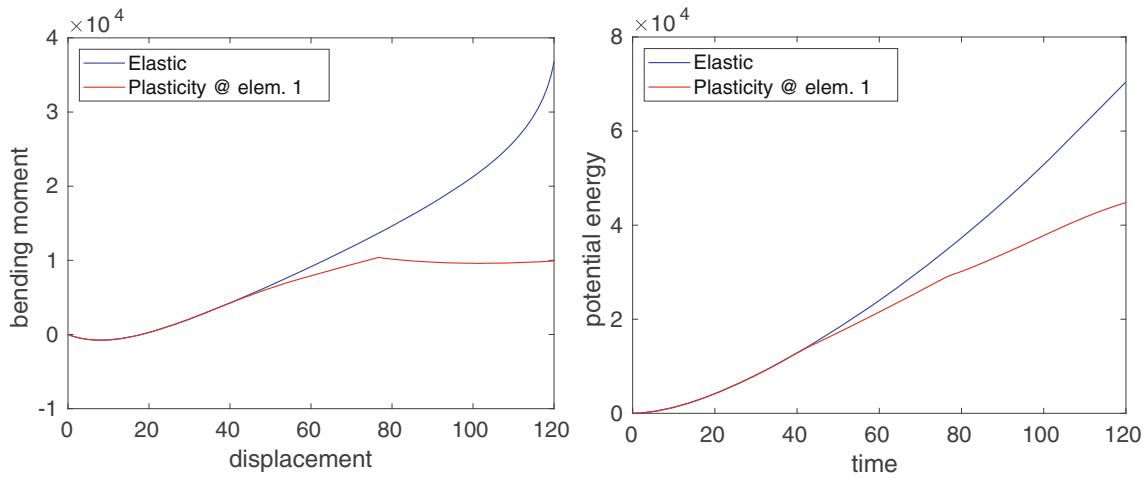


FIGURE 12 Circular arch: (left) Bending moment–Imposed displacement diagram near built-in end for elastic and plastic behavior (right) internal energy evolution for elastic and plastic case.

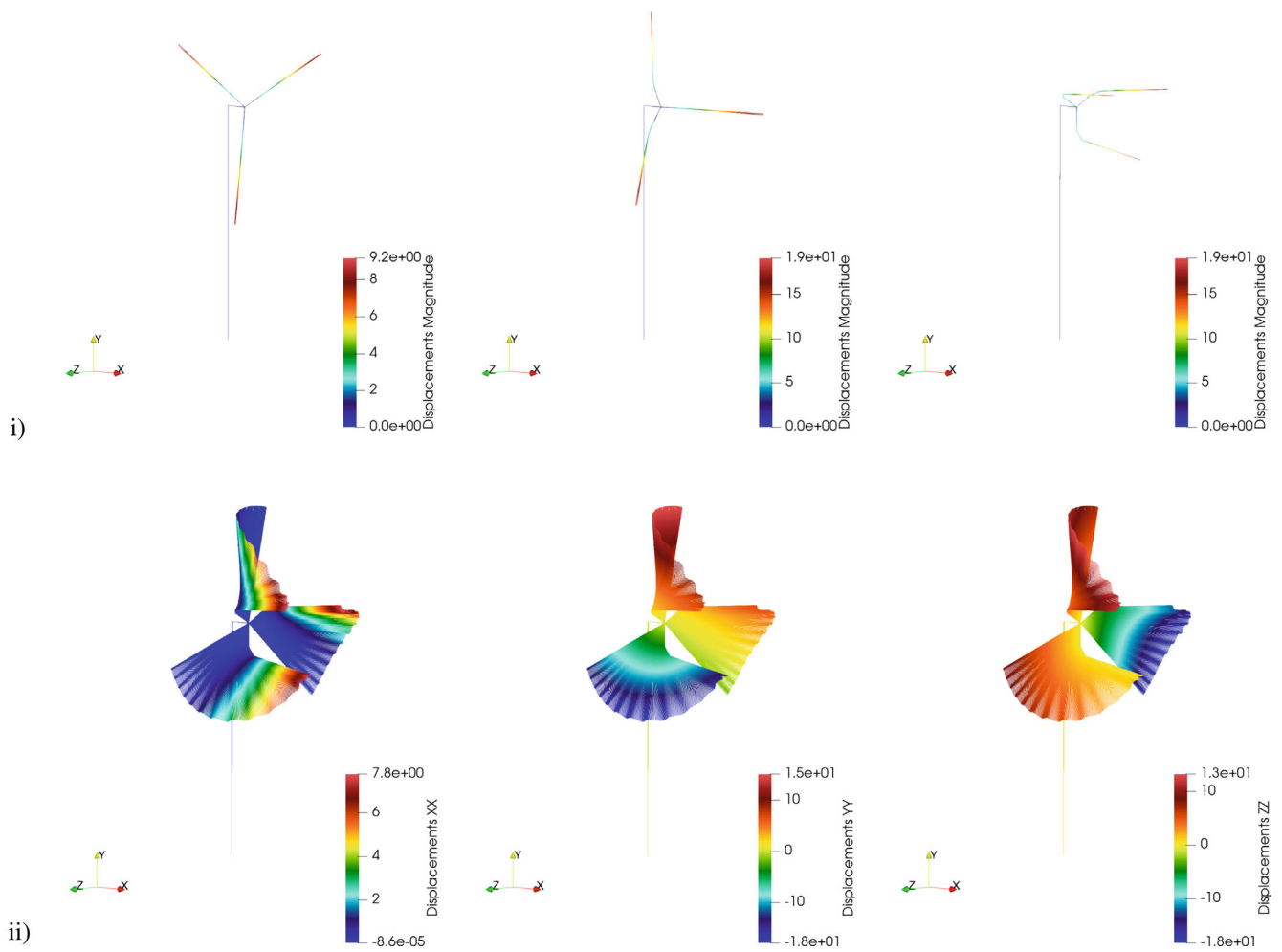


FIGURE 13 Wind turbine with flexible blades in localized failure: (i) Deformed shapes at time instants: $t = 0.3$ s, $t = 0.8$ s, $t = 1$ s; (ii) Evolution of displacement field components for $t \in [0.6, 1]$ s: x-direction, y-direction, z-direction.

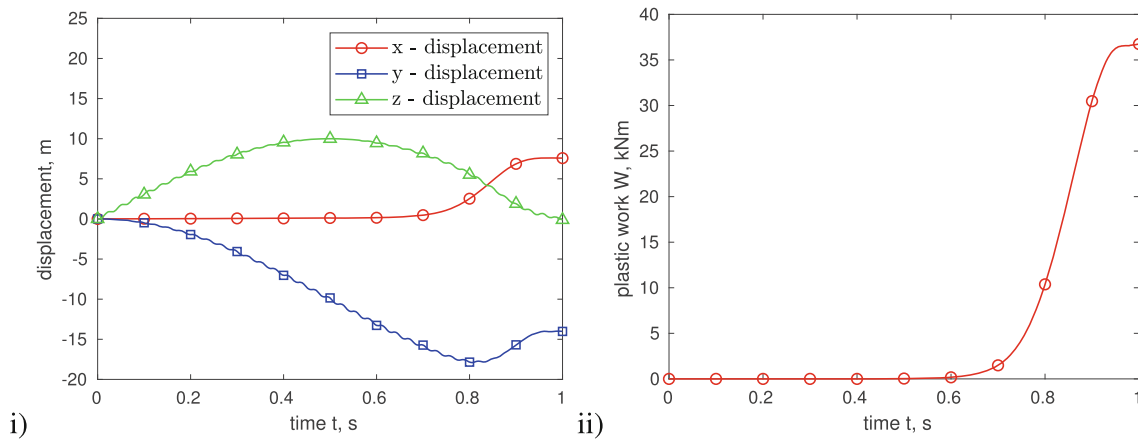


FIGURE 14 Wind turbine with flexible blades: (i) Displacement components at the blade tip; (ii) Accumulated plastic dissipation.

a 3D beam model development follows the same steps as those presented in this work for 2D version, other than dealing with a more complex non-vectorial character of 3D finite rotations.²⁴

We consider the wind turbine installation with three flexible blades, each with length $L = 10$ m. Here, we perform numerical simulation of such a rotating wind-turbine installation, when submitted to an extreme out-of-plane load (as simplification of extreme wind load) that triggers localized failure of flexible blades. More precisely, on each flexible blade, rotating with an angular velocity of $\omega = \pi$ rad/s, we also apply at the tip of the blade an out-of-plane point load $F = 2$ kN which increases in time $t \in [0, 1]$ until the localized failure is activated. Each beam element representing the blades is considered elastic, with the modulus of elasticity $E = 50$ GPa, apart the beam elements at the root of each blade with plastic behavior. Here we keep the same elastic modulus, along with the ultimate bending moment $M_u = 100$ MPa and the fracture energy $G_f = 50$ kNm. The computed response and subsequent deformed shapes for such a wind turbine system are presented in Figure 13. The blade tip displacement in all three directions are shown in Figure 14, along with the accumulated plastic dissipation that starts at approximately $t = 0.6$ s.

6 | CLOSING REMARKS

The presented geometrically exact planar beam model provides the ability to account for large elastic and plastic deformations, representing both the hardening and softening response phases. The proposed constitutive model considers finite deformation plasticity with a multiplicative split of deformation gradient, with regular part of plastic deformation in hardening and localized deformation in softening, along with the ability to reduce the stress resultants to zero at the beam fracture point. The plasticity criterion for hardening response can be constructed for any beam cross-section by following the procedure² resulting in the corresponding coupling between different stress resultants typical of beams.⁸ The softening response can be activated to model the fracture mode in the connections with different failure mechanisms. Which of these mechanisms will be activated depends on interplay and stress redistribution during the limit load analysis.

The proposed model development is optimized in many aspects. It requires non-local variational formulation, which allows us to introduce the main fracture parameter in terms of the fracture energy rather than (ill-defined) value of the characteristic length.¹¹ It also provides the dedicated embedded-discontinuity finite element approximation for modelling the fracture. Such a discrete approximation is optimal in the energy norm in the elastic phase, given the best approximation property of the finite element method. Moreover, the embedded-discontinuity finite element approximation also provides the best approximation of the dissipated energy, or dissipation. Thus, the proposed approach to fracture should be preferred to any other, if the quantity-of-interest is the plastic dissipation, both in the fracture process zone and in the final phase of crack coalescence (which jointly define the fracture energy), rather than a detailed representation of the crack kinematics.

The computational efficiency of the proposed model is enforced by the operator split computational procedure, which separates the global computations of nodal displacements/rotations and stress resultants from the computations in the local (element-wise) phase for internal variables including the crack opening. This (operator split) computational

procedure is illustrated here for homogeneous beams, but it can easily be generalized to heterogeneous beams at the cost of adding strain discontinuity by following our previous work on simple truss structures.²¹

By using the proposed beam element we can perform a comprehensive ultimate limit analysis for any slender frame undergoing large overall motion and including different failure mechanisms with large plastic deformation. The geometrically non-linear approach allows the ultimate limit analysis with large displacement without any need for a posterior correction.² This advantage is very important in any frame structure with a large ductility. The results for all numerical examples illustrate an excellent performance of the proposed beam element with mesh-invariance in softening computations.

Finally, the Reissner beam strain measures should be used carefully for large strain problems for high shear flexibility. Namely, it was observed³² that using the dual (material) normal force, which is normal to the section and not directed along the beam axis, and the elastic constitutive law in (26) can lead to an incorrect buckling load for compressed beams in the elastic case. However, this was not observed with the proposed plastic constitutive model proposed herein, which reduces the risk to obtain finite shear stress.

ACKNOWLEDGMENTS

This work was supported by the French National Research Agency (ANR, project MS3C), by IUF-Institut Universitaire de France (for AI) and the French Ministry of Europe and Foreign Affairs (MEAE, for SLj). All the financial supports are gratefully acknowledged.

DATA AVAILABILITY STATEMENT

The data that support the findings of this study are openly available in ASME Journal Applied Mechanics at https://asmedigitalcollection.asme.org/search-results?f_AllAuthors=R.+Schmidt, reference number 30. doi: <https://doi.org/10.1115/1.3423734>.

ENDNOTES

*Term 'geometrically exact beam' is introduced by Simo (see References 8,9) to denote that the beam model can represent large displacements and large rotations and provide the exact strain measures for beam theory regardless of their size; it should not be confused against 'exact geometry' representation by NURBS introduced in IGA; see Reference 10.

†All the developments to follow all apply to curvilinear beam axis and variable cross-section, with details presented in References 17,24. Here, one would have to introduce the rotation field to position the local frame in the beam initial configuration defined at each point of the beam axis $s \in [0, L]$, denoted as $\mathbf{g}_i = \mathbf{A}_0(s) \mathbf{e}_i$.

‡In embedded discontinuity discrete approximation we place localization point \bar{x} at the element Gauss point and limit the influence function support to one element only with $\tilde{G}^\epsilon(x)$ as the derivative of the corresponding shape function (e.g., see References 9,21,25). Namely, contrary to phase-field¹⁰ and non-local¹² models, the proposed embedded discontinuity finite element approach provides an element-wise approximation to the influence function, and thus does not require to specify so-called characteristic length.

§This requires that we first discretize the problem and then linearize, but in the present case, these two procedures can be inverted.⁷

¶It is easy to generalize to higher order approximation with a 3-node curved beam element.¹⁷

ORCID

Adnan Ibrahimbegovic  <https://orcid.org/0000-0002-6502-0198>

REFERENCES

1. Medic S, Dolarevic S, Ibrahimbegovic A. Beam model refinement and reduction. *Eng Struct*. 2013;50:158-169.
2. Dujc J, Brank B, Ibrahimbegovic A. Multi-scale computational model for failure analysis of metal frames that includes softening and local buckling. *Comput Methods Appl Mech Eng*. 2010;199:1371-1385.
3. Reissner E. On one-dimensional finite strain beam theory: the plane problem. *J Appl Math Phys*. 1972;23:795-804.
4. Ladeveze P. On reduced models in nonlinear solid mechanics. *Eur J Mech A/Solids*. 2016;60:227-237.
5. Chinesta F, Huerta A, Rozza G, Willcox K. Model reduction methods. In: Stein E, de Borst R, Hughes T, eds. *Encyclopedia of Computational Mechanics*. Vol 1. 2nd ed. Wiley; 2017.
6. Belytschko T, Song J. Coarse-graining of multiscale crack propagation. *Ing J Numer Methods Eng*. 2010;81:537-563.
7. Ibrahimbegovic A. *Nonlinear Solid Mechanics: Theoretical Formulations and Finite Element Solution Methods*. Springer; 2009.
8. Simo J, Hjelmstad DK, Taylor LR. Numerical formulations of elasto-viscoplastic response of beams accounting for the effect of shear. *Comput Methods Appl Mech Eng*. 1984;42:301-330.
9. Ibrahimbegovic A, Mejia-Nava RA. *Structural Engineering: Models and Methods for Statics, Instability and Inelasticity*. Springer; 2023.
10. Borden M, Verhoosel C, Scott M, Hughes T. A phase-field description of dynamic brittle fracture. *Comput Methods Appl Mech Eng*. 2012;280:217-220.

11. Bazant Z, Lin F. Non-local yield limit degradation. *Int. J. Numer Methods Eng.* 1988;26:1805-1823.
12. Jirasek M. Nonlocal models for damage and fracture: comparison of approaches. *Int. J. Solids Struct.* 1998;35:4133-4145.
13. Bourdin B, Francfort G, Marigo J. Numerical experiments in revisited brittle fracture. *J Mech Phys Solids.* 2000;46:1319-1342.
14. Griffith A. The phenomena of rupture and flow in solids. *Philosophic Trans R Soc London.* 1921;221:163-198.
15. Moes N, Belytschko T. X-FEM, de nouvelles frontieres pour les elements finis. *Revue Europeenne Des Elements Finis.* 2002;11:305-318.
16. Hughes T. *The Finite Element Method: Linear Static and Dynamic Analysis.* Prentice-Hall; 1987.
17. Ibrahimbegovic A, Frey F. Finite element analysis of linear and nonlinear planar deformations of elastic initially curved beams. *Int J Numer Methods Eng.* 1993;36:3239-3258.
18. Lubliner J. A maximum-dissipation principle in generalized plasticity. *Acta Mech.* 1984;52:225-237.
19. Tojaga V, Gasser T, Kulachenko A, Ostlunda S, Ibrahimbegovic A. Geometrically exact beam theory with embedded strong discontinuities for the modeling of failure in structures. Part I: formulation and finite element implementation. *Comput Methods Appl Mech Eng.* 2023;140:116013.
20. Ibrahimbegovic A, Wilson E. A modified method of incompatible modes. *Commun Numer Methods Eng.* 1991;7:187-194.
21. Ibrahimbegovic A, Melnyk S. Embedded discontinuity finite element method for modeling of localized failure in heterogeneous materials with structured mesh: an alternative to extended finite element method. *Comput Mech.* 2007;40:149-155.
22. Imamovic I, Ibrahimbegovic A, Mesic E. Coupled testing-modeling approach to ultimate state computation of steel structure with connections for statics and dynamics. *Coupled Syst Mech.* 2018;7:555-581.
23. Brank B, Korelc J, Ibrahimbegovic A. Nonlinear shell problem formulation accounting for through-the-thickness stretching and its finite element implementation. *Comput Struct.* 2002;80:699-717.
24. Ibrahimbegovic A, On FE. Implementation of geometrically nonlinear Reissner's beam theory: three-dimensional curved beam elements. *Comput Methods Appl Mech Eng.* 1995;122:11-28.
25. Ibrahimbegovic A, Brancherie D. Combined hardening and softening constitutive model of plasticity: precursor to shear slip line failure. *Comput Mech.* 2003;31:88-100.
26. Stakgold I. *Green's Function and Boundary Value Problems.* Wiley; 1979.
27. Marsden J, Hughes T. *Mathematical Foundations of Elasticity.* Dover; 1994.
28. Zienkiewicz O, Taylor R. *The Finite Element Method.* Vol I, II, III. Butterworth-Heinemann; 2000.
29. Taylor R. *FEAP-Finite Element Analysis Program.* University of California. <http://projects.ce.berkeley.edu/feap/>; 2014.
30. DaDeppo D, Schmidt R. Instability of clamped-hinged circular arches subjected to a point load. *ASME J Appl Mech.* 1975;97:894-896.
31. de Villede Goyet V, Frey F. Use of Marguerre theory in the nonlinear analysis of beam and plate structures. In: Robinson J, ed. *Proceedings 4th World Congress on FEM.* Robinson and Associates; 1984:456-462.
32. Kim MY, Mehdi A, Atar M. Finite strain theories of extensible and shear-flexible planar beams based on three different hypotheses of member forces. *Int J Solids Struct.* 2020;143-144:434-446.

How to cite this article: Ibrahimbegovic A, Mejia-Nava R-A, Ljukovac S. Reduced model for fracture of geometrically exact planar beam: Non-local variational formulation, ED-FEM approximation and operator split solution. *Int J Numer Methods Eng.* 2024;125(1):e7369. doi: 10.1002/nme.7369

APPENDIX. OPERATOR SPLIT COMPUTATIONAL PROCEDURE FOR LOCALIZED PLASTICITY

Local computation (for element e with rotation discontinuity):

$$\begin{aligned} \text{Given: } & \mathbf{d}_{n+1}^{e,(i)}, \alpha_n^e, h = t_{n+1} - t_n \\ \text{Find: } & \alpha_{n+1}^e, \text{ such that } \Phi_{n+1} \leq 0 \end{aligned} \quad (\text{A1})$$

We first test the elastic trial state produced with $\bar{\gamma}_{n+1}^{\text{trial}} = 0$:

$$\left. \begin{aligned} \bar{\gamma}_{n+1}^{\text{trial}} := \bar{\gamma}_{n+1}^{\text{trial}} h = 0 \\ \alpha_{n+1}^e = \alpha_n^e \end{aligned} \right\} \Rightarrow \begin{cases} t_{m,n+1}^{\text{trial}} = - \int_{L^e} \tilde{G}^T [EI (\sum_{a=1}^2 B_a^e d_{a,n+1}^{(i)} + \tilde{G}^e \alpha_n^e)] dx \\ \Phi_{n+1}^{\text{trial}} = |t_{m,n+1}^{\text{trial}}| - (M_u - q_n) \end{cases} \quad (\text{A2})$$

If the trial state produces a non-positive value of the yield function, $\Phi_{n+1}^{\text{trial}} \leq 0$, we accept the trial values as the final ones, including the incompatible mode parameter $\alpha_{n+1}^e = \alpha_n^e$. Hence, the only change of the traction force can come from a displacement increment:

$$\begin{aligned} \text{Lin}[t_{m,n+1}]_{\alpha^e} &:= t_{m,n+1} + \mathbb{K}_d \Delta d_{n+1}; \quad \mathbb{K}_d := \frac{\partial \bar{t}_m}{\partial \mathbf{d}} = EIB^T \\ \mathbb{K}_{\alpha^e} &:= \frac{\partial \bar{t}_m}{\partial \alpha^e} = 0 \end{aligned} \quad (\text{A3})$$

Alternatively, for a positive trial value of the yield function, $\Phi_{n+1}^{\text{trial}} > 0$, the elastic trial step is plastically inadmissible. We thus have to modify the incompatible mode parameter α_n^e to recover the plastic admissibility of the driving traction; namely, we first express the traction at discontinuity:

$$\begin{aligned} \bar{t}_{m,n+1} &= EI \left(\mathbf{Bd}_{n+1}^{(i)} + \tilde{G}^e \alpha_{n+1}^e \right) \\ &= EI \left(\underbrace{\mathbf{Bd}_{n+1}^{(i)} - \frac{1}{L^e} \alpha_n^e}_{\bar{t}_{m,n+1}^{\text{-trial}}} \right) - \frac{EI}{L^e} \underbrace{(\alpha_{n+1}^e - \alpha_n^e)}_{\bar{\gamma}_{n+1} \text{sign}(\bar{t}_{n+1})} \\ &= \bar{t}_{m,n+1}^{\text{-trial}} - \frac{EI}{L^e} \bar{\gamma}_{n+1} \text{sign}(\bar{t}_{n+1}) \end{aligned} \quad (\text{A4})$$

and rewrite the yield function in terms of the corresponding modification of its trial value:

$$\begin{aligned} 0 = \Phi(\bar{t}_{m,n+1}, q_{n+1}) &:= |t_{m,n+1}| - (M_u - q_{n+1}) \\ &= \underbrace{|\bar{t}_{m,n+1}^{\text{-trial}}| - (M_u - q_n)}_{\Phi_{n+1}^{\text{trial}}} + (q_{n+1} - q_n) - \frac{EI}{L^e} \bar{\gamma}_{n+1} \end{aligned} \quad (\text{A5})$$

For a linear softening law, where $q = -\bar{K} \alpha^e$ with a constant value of \bar{K} , we can express the last term in (A5) in terms of $\bar{\gamma}_{n+1}$:

$$q_{n+1} - q_n = -\bar{K} \bar{\gamma}_{n+1} \quad (\text{A6})$$

This allows us to obtain the final value of the plastic multiplier and update the incompatible mode parameter:

$$\bar{\gamma}_{n+1} = \frac{\Phi_{n+1}^{\text{trial}}}{\left(\frac{EI}{L^e} + \bar{K} \right)}; \quad \alpha_{n+1}^e = \alpha_n^e + \bar{\gamma}_{n+1} \text{sign}(\bar{t}_{m,n+1}^{\text{-trial}}) \quad (\text{A7})$$

For a nonlinear softening law, the result equivalent to (A7) ought to be obtained iteratively, according to:

$$\begin{aligned} (j) &= 1, 2, \dots \\ \text{as long as: } \phi_{n+1}^{(j)} &:= \phi_{n+1}^{\text{trial}} - \frac{EI}{L^e} \bar{\gamma}_{n+1}^{(j)} + \left[\hat{q}(\alpha_{n+1}^{e,(j)}) - \hat{q}(\alpha_n^e) \right] > 0 \ (\approx \text{tol.}) \\ \Rightarrow \text{Lin}[\phi_{n+1}^{(j)}] &:= \phi_{n+1}^{(j)} + D_{\bar{\gamma}} \phi_{n+1}^{(j)} \Delta \bar{\gamma}_{n+1}^{(j)} \\ \bar{\gamma}_{n+1}^{(j+1)} &= \bar{\gamma}_{n+1}^{(j)} + \Delta \bar{\gamma}_{n+1}^{(j)}; \quad \alpha_{n+1}^{e,(j+1)} = \alpha_{n+1}^{e,(j)} + \Delta \bar{\gamma}_{n+1}^{(j)} \text{sign}(\bar{t}_{m,n+1}^{\text{trial}}) \\ (j) &\leftarrow (j+1) \end{aligned} \quad (\text{A8})$$

In a plastic step, the corresponding value of the elasto-plastic tangent modulus can be written as:

$$\mathbb{K}_{\alpha} := \frac{\partial \bar{t}_m}{\partial \alpha} = \bar{K} \text{sign}(\bar{t}_{m,n+1}^{\text{trial}}); \quad \mathbb{K}_d := \frac{\partial \bar{t}_m}{\partial \mathbf{d}} = 0 \quad (\text{A9})$$

Having obtained the final value of incompatible mode parameter α_{n+1}^e , we carry on with

Global computation iterative sweep:

$$\begin{aligned}
 &\text{Given: } \mathbf{d}_{n+1}^{(i)}, \alpha_{n+1}^e, \text{ with } h_{n+1}^e(\mathbf{d}_{n+1}^{(i)}, \alpha_{n+1}^e) = 0 \\
 &\text{as long as: } \left\| \hat{\mathbb{A}}_{e=1}^{n_{elem}}(\hat{\mathbf{f}}^{e,int}(\mathbf{d}_{n+1}^{(i)}, \alpha_{n+1}^e) - \mathbf{f}^{e,ext}) \right\| > 0 (\approx \text{tol.}) \\
 \Rightarrow & 0 = \text{Lin} \left[\hat{\mathbb{A}}_{e=1}^{n_{elem}}(\hat{\mathbf{f}}^{e,int}(\mathbf{d}_{n+1}^{(i)}, \alpha_{n+1}^e) - \mathbf{f}^{e,ext}) \right] \\
 & \quad := \hat{\mathbb{A}}_{e=1}^{n_{elem}}(\hat{\mathbf{f}}^{e,int}(\mathbf{d}_{n+1}^{(i)}, \alpha_{n+1}^e) - \mathbf{f}^{e,ext}) + \left[\hat{\mathbb{A}}_{e=1}^{n_{elem}} \hat{\mathbb{K}}_{n+1}^{e,(i)} \right] \Delta \mathbf{d}_{n+1}^{(i)} \\
 & \mathbf{d}_{n+1}^{(i+1)} = \mathbf{d}_{n+1}^{(i)} + \Delta \mathbf{d}_{n+1}^{(i)}
 \end{aligned} \tag{A10}$$

where $\hat{\mathbb{K}}_{n+1}^{e,(i)}$ is the tangent stiffness of an element with discontinuity needed for the assembly of linearized form of the system in (A10); the is defined according to:

$$\begin{aligned}
 \text{Lin}[\mathbf{f}^{e,int}(\mathbf{d}_{n+1}^{(i)}, \alpha_{n+1}^e) - \mathbf{f}^{e,ext}] &= \mathbf{f}^{e,int}(\mathbf{d}_{n+1}^{(i)}, \alpha_{n+1}^e) - \mathbf{f}^{e,ext} + \mathbb{K}_{n+1}^{e,(i)} \Delta \mathbf{d}_{n+1}^{e,(i)} + \mathbb{F}_{n+1}^{e,(i)} \Delta \alpha_{n+1}^{e,(i)} \\
 \text{Lin}[h_{n+1}^e(\mathbf{d}_{n+1}^{(i)}, \alpha_{n+1}^e)] &= \underbrace{h_{n+1}^e(\mathbf{d}_{n+1}^{(i)}, \alpha_{n+1}^e)}_{=0} + \mathbb{F}_{n+1}^{e,(i),T} \Delta \mathbf{d}_{n+1}^e + \mathbb{H}_{n+1}^{(i),e} \Delta \alpha_{n+1}^e + \mathbb{K}_d \Delta \mathbf{d}_{n+1}^e + \mathbb{K}_\alpha \Delta \alpha_{n+1}^e
 \end{aligned} \tag{A11}$$

where the element matrices can be written explicitly:

$$\mathbb{K}_{n+1}^e = \int_{\Omega^e} \bar{\mathbb{B}}^{e,T} \mathbb{C}_{n+1} \bar{\mathbb{B}}^e dx; \quad \mathbb{F}_{n+1}^e = \int_{\Omega^e} \bar{\mathbb{B}}^{e,T} \mathbb{C}_{n+1} \tilde{\mathbb{G}}^e dx; \quad \mathbb{H}_{n+1}^e = \int_{\Omega^e} \tilde{\mathbb{G}}^{e,T} \mathbb{C}_{n+1} \hat{\mathbb{G}}^e dx \tag{A12}$$

The right choice of matrices \mathbb{K}_d and \mathbb{K}_α in (A11) is made according to (A3) for elastic or to (A9) for plastic step. With the residual at discontinuity equal to zero (given converged value of the incompatible mode parameter $\bar{\alpha}_{n+1}^e$), we can carry out the static condensation to reduce the size of the tangent stiffness matrix to obtain the standard format for the finite element assembly:

$$\underbrace{\left[\mathbb{K}_{n+1}^{e,(i)} - \mathbb{F}_{n+1}^e (\mathbb{H}_{n+1}^e + \mathbb{K}_\alpha)^{-1} (\mathbb{F}_{n+1}^{e,T} + \mathbb{K}_d) \right]}_{\hat{\mathbb{K}}_{n+1}^e} \Delta \mathbf{d}_{n+1}^{e,(i)} = \mathbf{f}_{n+1}^{e,ext} - \mathbf{f}_{n+1}^{e,int,(i)} \tag{A13}$$